Escola de Camins
Escola Tècnica Superior d'Enginyeria de Camins, Canals i Ports
UPC BARCELONATECH

TREBALL FINAL DE GRAU

Beach recovery capacity along Catalan beaches

Treball realitzat per:
Alex Rojals Mainar

Dirigit per:
Vicente Gracia Garcia

Grau en:
Enginyeria Civil

Barcelona, **setembre de 2016**

Departament d'**Eng. Hidràulica, Marítima i Ambiental**

ACKNOWLEDGEMENTS

In the first place, I would like to thank Vicente Gracia, for being my tutor and supervisor through this study despite the distance and the incompatibility of agendas. Also, I would like to appreciate all the people and institutions that have contributed in some way throughout this work, with documents, data, information and advice.

Thanks to the Institut Cartogràfic I Geològic de Catalunya (ICGC) for providing morphological data and Organismo Publico Puertos del Estado, Ministerio de Fomento, for offering important information on sea records.

A special thank to all the support I was given, particularly to my family who had always been there helping me throughout my academic career and guiding me to keep on fighting for what I like to study. Finally, I also want to make recognition to Enric Consegal, Alex Muchinik, Joan Quer and Maria Vallejo for being there every day, far away from home, and for the mutual support through this work, as well as all my friends who always believed in me.

ABSTRACT

Throughout the present study, sea and beach conditions along the Catalan coast is analyzed to calculate the capacity of waves to induce an onshore/offshore sediment transport. Results will serve to evaluate the capacity of beaches to recover the original shape after the pass of an extreme event.

Firstly, basic coastal theory is reviewed, analyzing the elementary forces and actions applied on the beach and sea bottom that generate a sediment transport. For a better understanding, beach and near shore morphological properties are examined, such as types of profiles, bar generation and nourishment or protection options. With it, 5 different parameters are studied in order to estimate the landward or seaward sediment transport.

Considering all the recorded wave data through the coast of Catalonia, the 5 different predictive formulations are evaluated, offering the possibility to compare their behaviors and relations to predict the evolutionary state of each of the beaches. From the final solutions we will be able to analyze the effectiveness of every parameter and link together all the variables involved.

CONTENTS

LIST OF FIGURES:

LIST OF TABLES:

1. Introduction

Sediment transport in oceans, seas, lakes and rivers occurs constantly due to fluid motion such as tides, wind and waves. The forces created by these motion result in an almost continuous movement of sand, either in suspension in the water column or in flows at the surface of the seafloor. Mainly for oceans and seas, it is well differentiated at the offshore and nearshore, the latter being the most important under a large number of coastal engineering scenarios of interest. A vector with both longshore and cross-shore components dominates transport on the nearshore zone. The longshore sediment transport component controls relatively long-term systematic profile changes and has been studied for approximately five decades, but there is still considerable uncertainty in many aspects such as the effects of grain size or barred topography. Cross-shore sediment transport studies are relatively recent, so uncertainty in prediction capability may be considerably greater.

Cross-shore sediment transport involves both offshore transport, creating an eroded beach profile such as occurs during storms or winter periods, and onshore transport, which derives to accretion profiles, dominating during mild wave activity or summer periods. Offshore transport tends to be a much rapid and regular process with transport more or less in phase over the entire active profile. Onshore sediment transport often occurs to take place as individual packets of sand moving onshore, widening the dry beach. This motion phenomenon is denoted to as “ridge-and-runnel” system.

Eroded beach profiles are characterized by a flat foreshore but also by an offshore bar resulting from the accumulation of eroded sediment. Sediments are lifted by turbulence at the breaking zone and transported offshore by the undertow current, which loses intensity as it enters the sea, creating huge accumulation of sediments called bars. The bar will act as an energetic filter itself, causing high waves to break but allowing smaller ones go beyond without breaking. The surpassing smaller waves will break closer to the shore, generating another or various smaller bars or even by a feedback effect growing bigger the existing one.

Ideally bars are not present in an accretive profile but instead there is an accumulation of sediments on the emerged part of the beach, caused by the onshore transport of sand, known as berms. In this situation slope tends to be steeper.

Intermediate cases may be considered too, such that offshore sediment transport takes place just after wave breaking, whereas onshore net sediment transport happens in the surf zone. Consequences for that hypothetic scenario might be the formation of both a berm and a bar, relatively smaller to the previous extreme cases.

THEORETICAL PART

2. Forces acting within the near-shore

Sediment transport is governed by different forces originated either by waves, wind or tides. These forces may be onshore or offshore directed, terminologically denoted as constructive or destructive forces, respectively, or even some forces can behave as constructive or destructive under certain conditions. In equilibrium, all acting forces are in balance and the profile remains more or less static, although there is always motion of the individual sand grains under even low wave activity. When hydrodynamic conditions change, one or more forces are modified and the equilibrium balance is broken, resulting in sediment transport gradients and profile changes. As we can observe, constructive forces are those that tend to produce onshore sediment transport, whereas destructive forces cause offshore sediment transport.

A first onshore-directed force is to be considered due to the oscillatory water particle velocities. Although the time mean of the water particle velocity is zero, the sinusoid motion generates an average bottom shear stress τ_b at the nearshore zone, expressed as:

$$\overline{\tau_b} = \rho \frac{f}{8} \overline{|v_b| v_b}$$

where ρ is the mass density of water, *f* the Darcy-Weisbach friction coefficient and v_b the instantaneous wave-induced water particle velocity at the bottom.

A second constructive force originates within the bottom boundary layer, which causes a net mean velocity in the direction of propagating water waves. Induced by the streaming velocity, the bottom shear stress τ_{bs} is given by:

$$\tau_{bs} = -\frac{\rho \, \epsilon^{\frac{1}{2}} \sigma^{\frac{3}{2}} H^2 \, k}{8\sqrt{2} \, \sinh^2 kh}$$

in which , ϵ is the eddy viscosity, ρ is the mass density of water, σ the wave angular frequency, k the wave number, H the wave height and h the depth.

At the surf zone, cross-shore sediment transport is predominant due to sediment in suspension. Turbulence, although it is not a true force, lifts up sediment that may be transported shoreward or seaward depending on the water particle velocity. In 1973 Dean noted that the direction of cross-shore transport is determined by the distance of the suspended particle above the sea bottom and the fall velocity *w*. The time required for that grain particle to fall back to the bottom, if the sediment particle is suspended a distance above the bottom proportional to the wave height *H*, is

proportional to *H/w*. Although it is a an overly simplistic approach, he then realized that whether the fall time is less than $\frac{1}{2}T$ the particle should experience net onshore motion, whereas for higher values it would tend to move seawards.

The major destructive force is the undertow current, a seaward return flow of wave mass transport. It induces a stress on the bottom sediment particles and affects the suspended load. Suspended sand concentration is higher near the seabed, where undertow it the main current, thus sediments would be dragged offshore.

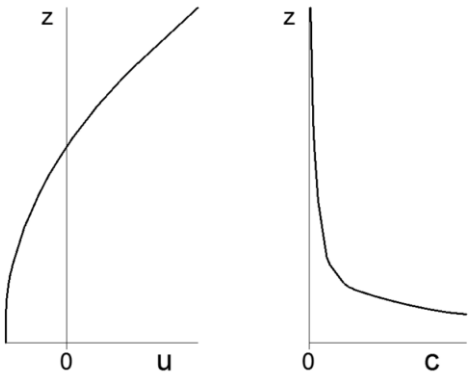

Figure 1: Water flow profile (left), and suspended sediment concentration profile (right)

The seaward discharge due to the return flow of shoreward mass transport *Q* is quantified as:

$$Q = \frac{E}{\rho\, C}$$

where *E* is the wave energy density and *C* is the wave celerity.

Another destructive force associated to the shoreward flux of linear momentum induced by with the wave propagation. The momentum is transferred to the water column when waves break inducing an equivalent shear force on the water. This causes a seaward bottom shear stress within the breaking zone.

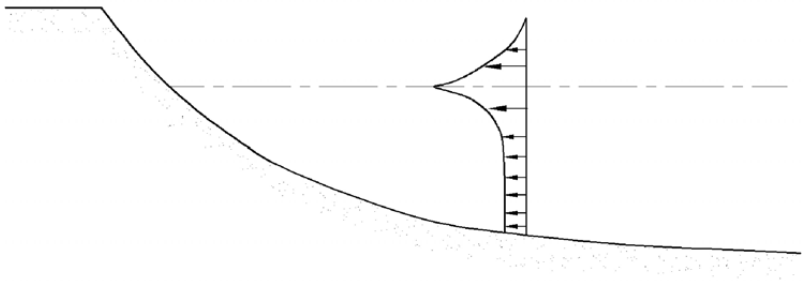

Figure 2: Distribution of the flux of onshore component of momentum. ***Font: CEM Part III chapter 3***

By the effect of strong winds and the surface wind stress τ_η, a closed loop current is originated, having a flow on the same direction as the wind at surface but a contrary directed bottom flow. Therefore, landward and seaward-directed winds will result in destructive forces and constructive forces, respectively.

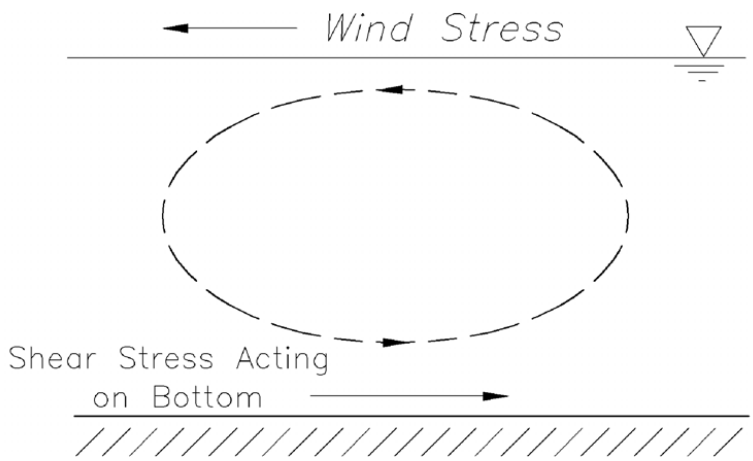

Figure 3: Shear bottom stresses caused by wind. ***Font: CEM Part III chapter 3***

Under linear wave theory, and a linear shear stress relationship with eddy viscosity, the distribution of the mean velocity over depth for the case of return of mass transport, considering the last three commented effects, is shown to be:

$$v(z) = \frac{h}{\rho\epsilon}\left[2\tau_\eta - \frac{\partial E}{\partial y}\right]\left[\frac{3}{8}\left(\frac{z}{h}\right)^2 + \frac{1}{2}\left(\frac{z}{h}\right) + \frac{1}{8}\right] + \frac{3}{2}\frac{Q}{h}\left[1 - \left(\frac{z}{h}\right)^2\right]$$

The first term is related to the surface wind stress τ_η and so to the wind effect. The second term, expressed as a function of the cross-shore gradient in wave energy $\frac{\partial E}{\partial y}$, is linked to the vertical gradient of momentum flux. It can be noted that the momentum flux only contributes inside the surf zone, where energy is dissipated, since outside the breaking point it is zero. Finally the third term is associated with the seaward return flow of mass transport, thus the undertow current.

The shear stress associated with the vertical velocity distribution generated under the three effects contemplated, can be calculated for any elevation as:

$$\tau = \rho\epsilon\,\frac{\partial v}{\partial z}$$

where , ϵ is the turbulent eddy viscosity. The resultant offshore-directed bottom shear stress, $z = -h$, is thus computed as:

$$\tau_b = \frac{1}{4}\frac{\partial E}{\partial y} - \frac{\tau_\eta}{2} + 3\,\frac{\epsilon E}{Ch^2}$$

We should also take into consideration the effect of the gravity force, which is mostly a destructive one. It acts down slope, therefore is generally seaward directed for a monotonic profile, though in presence of a bar, it may turn as an accretive force over little portions of the profile. Gravity serves as a stabilizing force if other forces are applied, however if it were the only force, the equilibrium profile solution would be no other than a horizontal, making it impossible for sandy beaches to exist.

The different forces and actions discussed above are reflected in Table 1, giving a general approximation of their magnitude for breaking and nonbreaking waves. Calculations were made considering an equilibrium profile with D=0.2m, H=0.78m, h=1.0m, T=8s and a wind speed of 20m/s.

	Description of Action	**Magnitude of Force (N/m2)**	
		Breaking Waves	Nonbreaking Waves
Constructive	Average Bottom Shear Stress Due to Nonlinear Waves (τ_b) for f=0.08	0.84	
	Streaming Velocities	28.9	
	Overtopping	28.6	
Destructive	Gravity	0.046	
	Undertow Due to Mass Transport	28.6	
	Undertow Due to Momentum Flux Transfer	7.9	0
Constructive or Destructive	Wind Effects	0.95	
	Turbulence	Relatively Large	Relatively Small

Table 1: Classification, between constructive or destructive, of all the acting forces and their magnitude values.
Font: CEM Part III chapter 3

3. Beach profile change predictors by simple parameters

3.1 Dean's number

Using small-scale laboratory data, in 1973 Robert G. Dean, managed to suggest a formula that discriminated between erosive and accretive profiles. He took into account the basic assumption that sediment was suspended during the wave crest phase position, so if the fall time was less or greater than one half of the period, the net transport would be landward or seaward, respectively.

He correlated deep water wave steepness to the fall velocity parameter and reached the following discrimination formula:

$$\frac{H_0}{L_0} = c_1 \frac{\pi w_f}{gT}$$

where c_1 is estimated as a constant 1.7 value and w_f being the fall velocity of the sediment suspended in still water. Values of wave steepness smaller than the one that fulfills the condition means low wave energy period and thus will tend to an accretive and berm profile. Instead, greater values of wave steepness will represent a storm and bar profile, therefore a seaward net sediment transport.

Considering linear theory representation of deep water wave length as $L_0 = \frac{gT^2}{2\pi}$, we can rearrange the previous expression to the dimensionless Dean's Number parameter:

$$\Omega = \frac{H_0}{w_f T} \rightarrow \ \Omega = \mathrm{c}_2 = \frac{c_1}{2} = 0.85$$

Values of the Dean's Number greater than 0.85 will lead to an erosive profile, while smaller values would tend to generate an accretive profile.

In 1986, Kriebel, Dally and Dean, re-examined with newer and more reliable values, consisting only on prototype and large-scale laboratory data, and realized that the constant proposed by Dean (1973) was approximately 2.8 rather than 0.85.

3.2 Hattori and Kawamata

Hattori and Kawamata in 1981 suggested a new correlation of factors, this time based also on the relationship, found by Thornton in 1987, between the ratio of the turbulent velocity intensity to the wave-induced velocity intensity and the surf similarity parameter $\xi_0 = tan\beta \sqrt{H_0/L_0}$. The beach slope, represented by the tangent of the angle β, can be measured as the average slope to the breaking point, $tan\beta = h_b/x_b$, being h_b and x_b the breaking depth and the breaking distance to the shore, respectively.

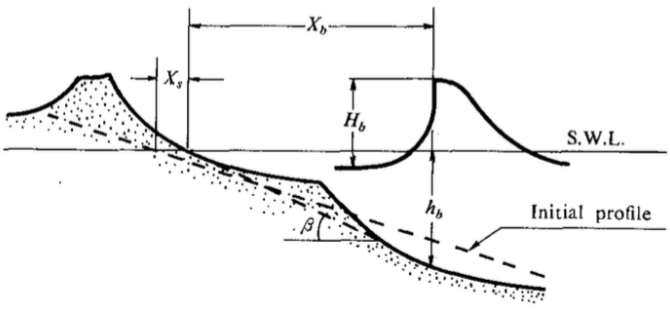

Figure 4: Sketch of the beach profile. ***Font: CEM Part III chapter 3***

The turbulence generated by breaking waves acts as a stirring agent for suspending sediment particles. Based on Thornton's results, the stirring power P_S can be written as:

$$P_S = a' \, W \, \hat{u} \, tan\beta$$

where *W* is the submerged weight of sand grains and $\hat{u}$ the maximum wave-induced velocity. By means of the linear long wave theory, the maximum wave-induced velocity is expressed as: $\hat{u} = 2\pi \left(\frac{H_b}{L_b}\right) gT$, H_b and L_b being the wave height and length at the breaking position. With that, we can rearrange the previous stirring power formula as:

$$P_S = a'' \, W \left(\frac{H_b}{L_b}\right) gT \, tan\beta$$

in which *a''* is a constant.

On the other hand, considering the gravitational force as its major agent, the resisting power against lifting sand grains from the bottom was found as:

$$P_R = a'''W \, w_S(d)$$

where $w_S(d)$ is the fall velocity depending on the sand grain diameter *d* and *a'''* is a constant.

Once again, if the stirring power P_S is greater than the resisting power P_R, sand grains would tend to keep in suspension due to the breaking waves, and then, transported seaward by wave-induced currents. Otherwise, sand grains are lead to roll and jump on the bottom surface if the resisting power is greater than the stirring one. For this case, sand is shifted shoreward through the bottom bed. Concluding, the net sediment transport direction can be shown as the ratio of the two powers described above:

$$\frac{H_b/L_b \, tan\beta}{w_s(d)/(gT)} \begin{cases} < C' & Onshore \; transport \\ = C' & Neutral \\ > C' & Offshore \; transport \end{cases}$$

C' is a constant that has to be determined by laboratory and field data, but at it is well known, under breaking conditions it is hard to measure wave and sediment progressions within the surf zone. Assuming that breaking wave steepness is related to deep-water wave steepness, much easier to determine, Hattori and Kawamata proposed a modification of the latest relation ratio between resisting and stirring powers:

$$\frac{H_0/L_0\ tan\beta}{w_s(d_{50})/(gT)} \begin{cases} < C & Onshore\ transport \\ = C & Neutral \\ > C & Offshore\ transport \end{cases}$$

C is a constant based on deep-water values from laboratory and field data. It is noticed that the expression that Hattori and Kawamata suggested is quite similar to the one proposed by Dean, but considering also the effect of beach slope. It should be noted that both the sediment fall speed and the beach slope tend to increase with increasing sand size. Therefore, the addition of the beach slope in the numerator tends to counteract to some extent the fall speed in the denominator.

Hattori and Kawamata performed a laboratory and field data research, based on this study, for recognizing an erosive or accretive beach profile and represented the results in terms of $(H_0/L_0)\ tan\beta$ and $w_S(d_{50})/gT$. From figure 5 it is perceived that the two different areas for an erosive and accretive profile, are distinctly separated by a line corresponding to the value of $C = 0.5$. Although there is a mixed region, defined by $0.3 < C < 0.7$, which is believed to being affected by the growth and reduction of breaking-point bars, which depends on the direction of bar migration propensity.

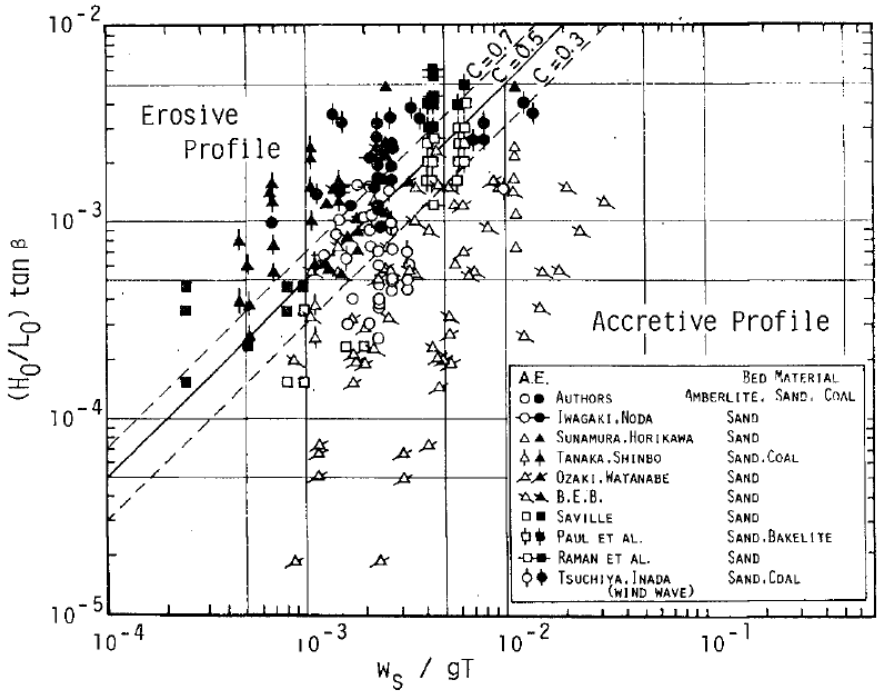

Figure 5: Classification of erosive and accretive beach profile. ***Font: Hattori and Kawamata (1981)***

3.3 Sunamura and Horikawa

Previously, in 1974, Sunamura and Horikawa already pointed out the difficulty in classifying and grouping beach profiles into bar and step types, as conventionally made, because of the tendency of bar and shoreline migration and complexity of the beach pattern. Considering plane profiles, they suggested a relationship to predict the beach response, based on small-scale laboratory data:

$$\frac{H_0}{L_0} = C(tan\beta)^{-0,27}\left(\frac{d}{L_0}\right)^{0.67}$$

Values of *C* for accretive or erosive characteristics were found by plotting the results under both conditions for different locations in terms of (H_0/L_0) and $(tan\beta)^{-0,27}(d/L_0)^{0.07}$. As it is revealed in Figure 6, for values of *C* greater than 8, we will be under erosive conditions, while for values lower than 4, an accretion profile will take place. Values in between show a transition zone.

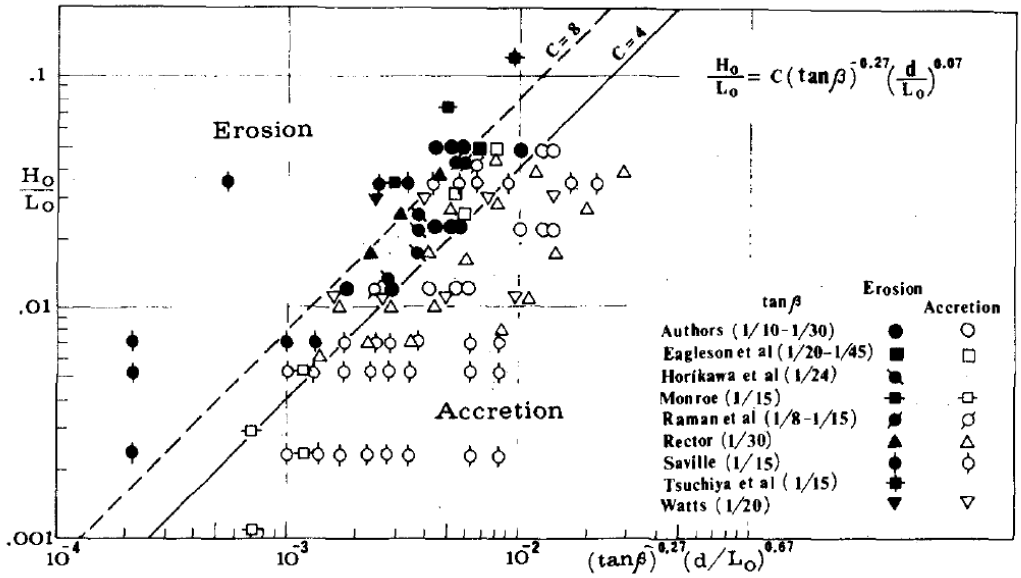

Figure 6: Classification of erosive and accretive beach profile for Sunamura and Horikawa. ***Font: Sunamura and Horikawa (1974)***

More recent researches of sediment movement in wave breaking point also obtained similar parameters, which made possible the distinction between erosion and accretion, such as the subsequent study of Sunamura (1980). Sunamura investigated and checked these parameters with newer and more reliable values.

Therefore, still based on the dimensionless parameter proposed by Sunamura and Horikawa (1974), he found out a new boundary between erosion and accretion, given by the line defined as:

$$\frac{H_0}{L_0} = 18(tan\beta)^{-0,27}\left(\frac{d}{L_0}\right)^{0.67}$$

The new redefinition defined the accretion processes as those for which $C < 18$, and erosive conditions for higher values, as seen in the figure below:

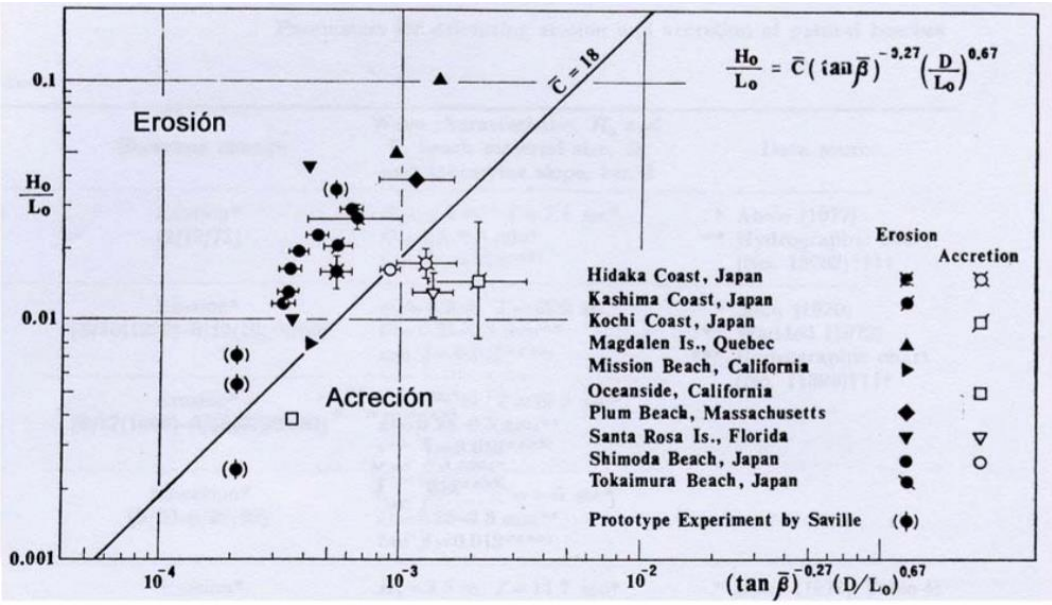

Figure 7: Delimitation of erosion or accretion. ***Font: Sunamura (1980)***

3.4 Ahrens' criteria

John Ahrens, in 1998, complementing the work done in 1987 by Zenkovich and Schwartz, suggested a different criterion based on the comparison of the stability number N_S to deep-water wave steepness H_{SO}/L_0. The dimensionless stability number parameter is defined as:

$$N_S = \frac{H_0}{\frac{\rho_s - \rho_w}{\rho_w} D_{50}}$$

where, ρ_s is the density of sediment and ρ_w the density of water.

Considering that $H \propto u_{max}^2$, Ahrens realized that the stability number was similar to Shields' initiation of motion parameter, and so by comparing both he determined that the curve that differentiated, in a better way, among erosion or accretion conditions, was the one corresponding to $u_t = -2$, being u_t the orbital maximum velocity at the wave trough. The erosion limiting condition corresponds to $u_t = -1.51$, defining exclusive accretion conditions for higher values of u_t. The $u_t = -1.51$ curve is shown to be as:

$$N_S = 30.8 \left(\frac{H_{SO}}{L_0}\right)^{-0.854} e^{10.1\left(\frac{H_{SO}}{L_0}\right)}$$

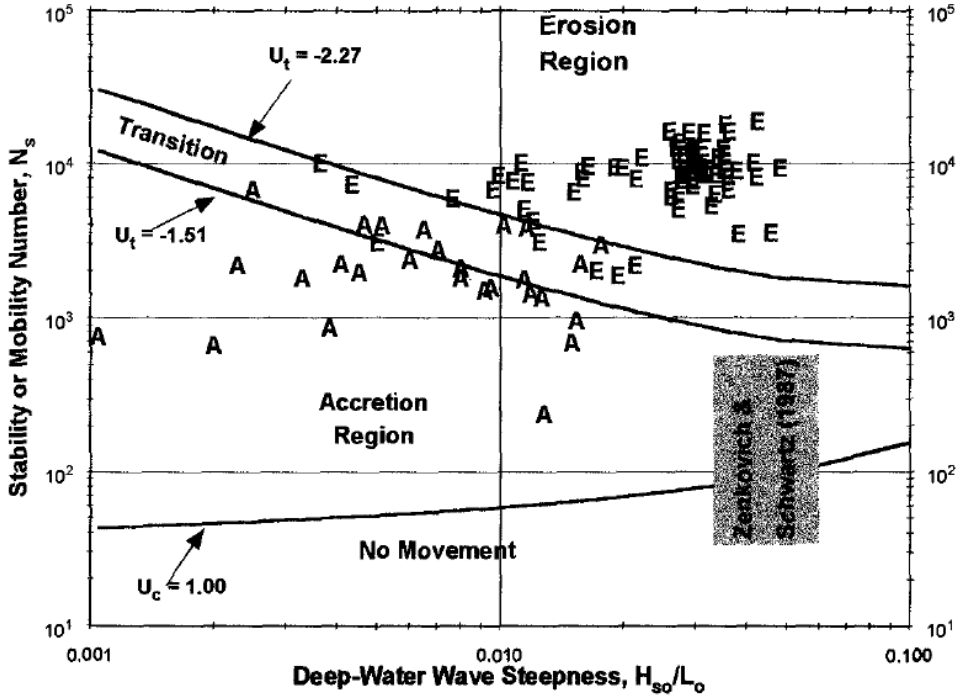

Figure 8: Classification of erosive and accretive beach profile for Ahrens' criteria. ***Font: Ahrens (1998), originally Zenkovich and Schwartz (1987)***

3.5 Ursell number

Several studies showed up that under nonbreaking conditions onshore sediment transport tends to be the dominant, produced basically by short wave skewness. Measurements held at barred beaches recall on the importance that some processes, such as wave skewness, had a direct relation with the bed-load net onshore transport.

It is known that a good prediction of wave skewness expression requires three independent variables, the Ursell number, the surf similarity parameter and the normalized wavelength. In a basic way though, we can rely all the importance for the forecast of the skweness on Ursell number only:

$$Ur = \frac{HL^2}{h^3}$$

For small values of the Ursell number, wave skewness and asymmetry are close to zero. Instead, when Ursell number increases, skewness increases first to a maximum and then decreases to zero, whereas wave asymmetry increases in magnitude but in negative values.

3.6 Predictors summary

All predictors are found summarized in the following table, as well as the discrimination value of each one of the adimensional variables:

Parameter	Formula	Discrimination Value	
		Accretive	Erosive
Dean's Number	$\Omega = \frac{H_0}{w_f T}$	$\Omega < 2.8$	$\Omega > 2.8$
Hattori and Kawamata	$HK = \frac{2H_0}{w_s(d_{50})\,T}\ tan\beta$	$HK < 0{,}5$	$HK > 0{,}5$
Sunamura and Horikawa	$\frac{H_0}{L_0} = C(tan\beta)^{-0{,}27}\left(\frac{d}{L_0}\right)^{0.67}$	$C < 18$	$C > 18$
Ahrens' Criteria	$Ah = N_S\left(\frac{H_{SO}}{L_0}\right)^{0.854} e^{-10.1\left(\frac{H_{SO}}{L_0}\right)}$	$Ah < 30.8$	$Ah > 30.8$
Dalrymple's Profile Parameter	$P = \frac{gH_o^2}{w_f^3 T}$	$P < 10000$	$P > 10000$

Table 2: Definition of predictor parameters and their typical discrimination value

4. Equilibrium Profiles and Bars

The concept of an equilibrium beach profile is quite simple, the absence of net cross-shore sediment transport because of the balance of many different forces acting, but it's not really long lasting since in nature the forces are always changing with the varying waves, currents, winds and tides. These changes will generate a disequilibrium causing cross-shore sediment transport. But still the idea of an equilibrium profile is one of the most valuable tools for coastal engineering to provide a framework to consider disequilibrium and thus cross-shore sediment transport.

Under the assumption that no long-shore gradients exist, cross-shore transport does not lead to net gain or loss of sediment, just a redistribution of sand across the profile. This let us assume the principle of conservation of sand across the profile for retreating and advancing equilibrium profiles. The total sand volume is conserved in the active zone, so for retreating profiles the erosion is located at the exposed beach face requiring a compensating deposition offshore, whereas for advancing profiles sediments are eroded in the surf zone and deposited on the exposed beach face. Supposing that there is a long-shore gradient in the sediment transport vector, there is a uniform advance or retreat of the profile at all active elevations, maintaining its shape across the profile and so sediments in volume can be added or removed from the profile without changing its shape. That is why most methods for predicting beach

profile changes tend to consider the two components of the vector separately, cross-shore and long-shore, determining the final profile form and location by superposition of both.

The shoreline position retreats abruptly during high wave events, such as storms and sea rises, and advances offshore, linear and gradually, on mild wave activity periods. Figure 9 represents the results from Katoh and Yanagishima of the shoreline position over a period of approximately 7 months, from March to September 1988, where it is clearly visible the abruptly retreat on a high wave energy flux and a shoreline advancement during the recovery phase that turns to be almost constant at 0.68m/day.

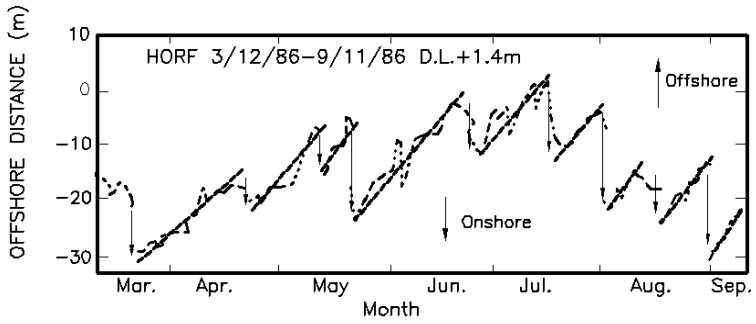

Figure 9: Shoreline position changes from March to September 1998. ***Font: CEM Part III chapter 3***

4.1 Long-shore bar formation and seasonal shoreline changes

Many beaches in nature present one or more long-shore bar, which may be seasonal or more or less permanent. Bars depend basically on wave and sediment conditions. Their formation is commonly associated with a seaward transport of sediment and a retreat of shoreline and can be affected and pushed farther seaward during storm periods. For a multiple bar beach, the inner bars will show to be more vulnerable to changing wave conditions than those offshore, since the outer bars may have been caused by a past large storm which dropped the sand in water too deep for normal weather conditions to return the sand to shore or to far deep for another storm to affect it.

Based on field observations, Dean already realized that if the fall time were less or greater than a half of the wave period, the net transport would be landward or seaward, resulting in bar formation in the latter case. He then proposed the following relationship for offshore sediment transport leading to bar formation:

$$\frac{H_o}{w_f T} \geq 0.85$$

where $H_o$is the deep water reference wave height. Later in 1991, Kraus, Larson and Kriebel suggested two more relationships for bar formation, under large wave tank data studies:

$$\frac{H_o}{L_o} \geq 115\left(\frac{\pi w_f}{gT}\right)^{\frac{3}{2}} \qquad \frac{H_o}{L_o} \leq 0.0007\left(\frac{H_o}{w_f T}\right)^3$$

Finally Dalrymple in 1992 recommended representing the two last equations in terms of a single profile parameter *P*, which for values exceeding about 10.000 would lead to bar formation, and so, to an eroding profile:

$$P = \frac{gH_o^2}{w_f^3 T}$$

4.2 Parameters of bars geometry

The bar geometry was defined by Keulegan (1945, 1948) after some studies both in laboratory and field data, which determined the relationships for bar formation. Keulegan defined the depth over the bar crest h_{CR}, the depth of the bar trough h_T and the depth to the bar base h_D at the position of the bar crest, as seen in the figure 10 below. He then stated that the ratio of depths of bar crest to bar base h_{CR}/h_D was approximately 0.58 for laboratory and field data. He also realized that the ratio between depth trough and crest h_T/h_{CR} oscillated from 1.6 to 1.8. Finally he identified that due to varying wave height and water levels in nature, laboratory bars are considerably narrower than those shaped in nature, the later being approximately twice as wide as the laboratory one.

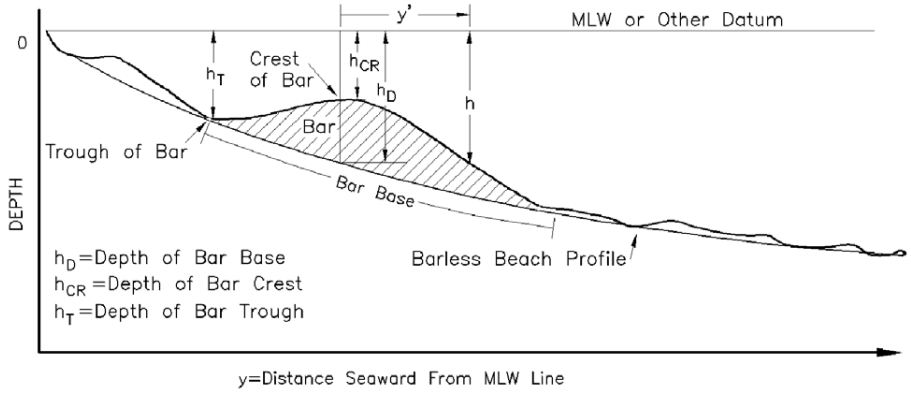

Figure 10: Offshore bar sketch. ***Font: CEM Part III chapter 3***

4.3 Equilibrium profiles

It is generally observed that equilibrium profiles tend to be concave upward. They also have milder slopes when composed of finer sediments and appear to have flatter slopes for steeper waves. Because of the cross-shore sediment transport, the sediments tend to be grouped with finer and coarser sediments residing in the deeper and shallower waters, respectively.

Numerous models have been suggested for representing equilibrium beach profiles (EBP). Dean at 1977 studied 3 cases of forms of EBPs that would result under different dominant destructive forces: wave energy dissipation per unit volume, wave energy dissipation per unit surface area and uniform average long-shore shear stress across the surf zone.

By using linear wave theory and a simple wave-breaking model, he found out that for all three destructive forces the EBP could be expressed by a simple algebraic form:

$$h(y) = A * y^n$$

in which *A* represents a sediment scale parameter. The exponent *n* was calculated to be 2/3 for the wave energy dissipation per unit volume case, and 0.4 for the other two cases. But after being studied approximately 500 profiles from the east coast and Gulf shorelines of the United States, the results show that although there was an extensive interval of values, 2/3 provided the best overall fit to the data.

Moore and Dean calculated empirical relationships between the sediment scale parameter *A* as a function of sediment size *D* and fall velocity w_f:

$$A(w_f) = 2.25 \left(\frac{w_f^2}{g}\right)^{\frac{1}{3}}$$

$$A(D_{50}) = \begin{cases} 0.41\ (D_{50})^{0.94}, D_{50} < 0.4mm \\ 0.23\ (D_{50})^{0.32}, 0.4mm < D_{50} < 10mm \\ 0.23\ (D_{50})^{0.28}, 10mm < D_{50} < 40mm \\ 0.46\ (D_{50})^{0.11}, 40mm < D_{50} \end{cases}$$

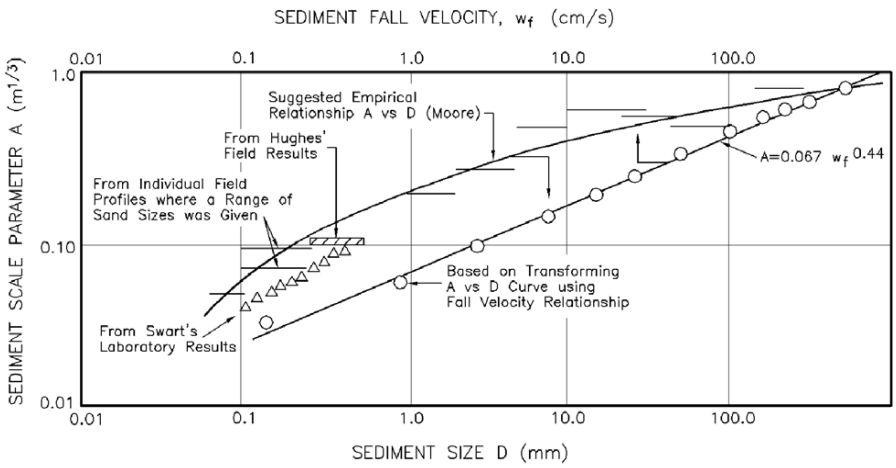

Figure 11: Variation of sediment scale parameter *A* with sediment fall velocity w_f and sediment size *D*. *Font: CEM Part III chapter 3*

The equation proposed by Dean can be seen as an approximation with two inherent limitations. At the water line (y=0) the slope of the beach profile is shown to be infinite, furthermore it represents a monotonic beach profile form, disregarding the possible existing bars. Fortunately by recognizing gravity as a destabilizing force the first limitation can be overcome. For it the beach face slope is denoted as m_o and the given equation transforms to:

$$y = \frac{h(y)}{m_o} + \left(\frac{h(y)}{A}\right)^{\frac{3}{2}}$$

Other more complex formulas were suggested such as an exponential beach profile proposed by Bodge in 1992:

$$h(y) = h_0\,(1 - e^{-ky})$$

where, h_0 is the asymptotic depth at a great offshore distance and *k* is a decay constant. This and other exponent formulas have two free constants that are determined to offer the best results that approximate the field data and so, they are more accurate than the Dean's first equation constrained to the *n*=2/3.

Occasionally, the beach profile can be approximated by an equilibrium compound profile, consisting on two simple parabolic profiles. One representing the surf zone with its origin at the dry beach at high tide and the other denominated the shoaling profile with its source at the low tide elevation but displaced in vertical, so that their intersection coincide with the breaking wave depth.

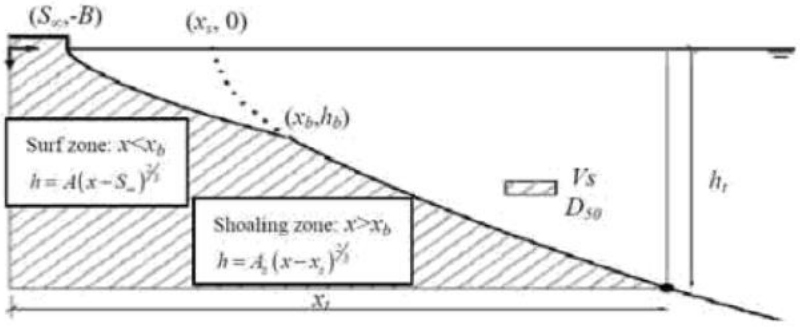

Figure 12: Bi-parabolic beach profile. ***Font: CEM Part III chapter 3***

5. Limits of cross-shore sand transport and equilibrium beach profile erosion model

The cross-shore sediment transportation is limited both in the onshore and offshore directions. The onshore limit of profile response represents the maximum raise and landward limit of sediment transport. This upper limit of sediment deposition is defined as a depositional beach berm during constructive conditions, in which beachfront shapes seaward. Under receding conditions, it's seen that the berm may retreat inland on a more or less uniform way. In those cases where the berm is high enough so that the run-up never reaches its crest, an erosion scarp may be formed above the run-up limit. The slope of the eroding scarp may be quite abrupt, even approaching vertical for some cases.

Short-term erosional events are characterized by high waves and elevated water levels. In this case, the seaward limit of interest is the significant quantity of sand sediments transported and deposited further offshore. The shallow areas of the profile are the most affected ones to this readjustment. If in storm surge the waves overtop the berm, and then over wash occurs, the landward limit is restricted by the individual uprush sediment transportation capacity. This boundary may be determined by the energy transportation loss due to seepage on the beach or by the impounded water due to the event itself.

In a basic way, cross-shore profile changes can be predicted by calculating the depth of limiting motion, referring to the limit to which the depositional front has advanced. Vellinga in 1983 already recommended this depth to be $0.75H_s$ where H_s is the deepwater significant wave height calculated from the breaking wave height.

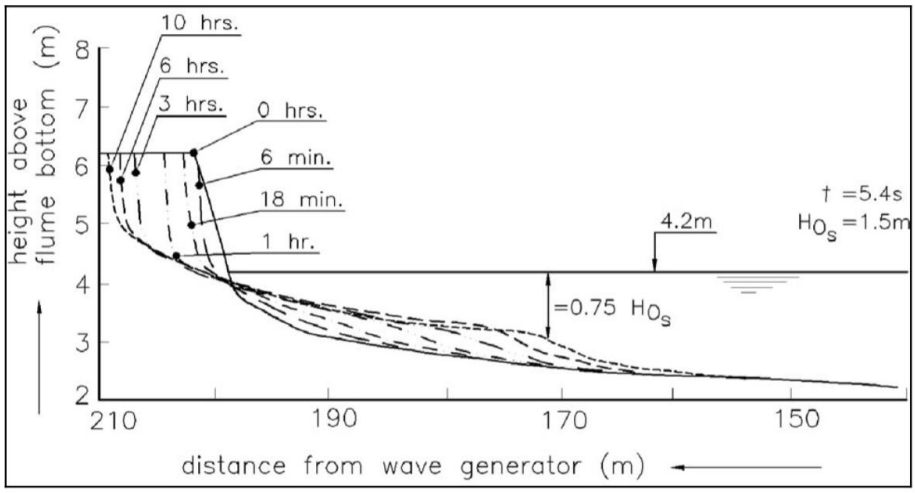

Figure 13: Erosional profil·le evolution, results from Vellinga 1983. ***Font: Vellinga (1983)***

Over long-term time scales, the seaward limit of effective profile, where no more significant effects are noted, is denoted to as the closure depth indicated by h_c or d_c. For the case where no field data is available and thus no empirical estimation can be done, Hallermeier in 1978, 1981 figured out the first approach to the finding of closure depth. He actually established two different depths, the shallowest determining the limit of intense bed activity and the deepest delineating the position where no or little sand transport due to waves is expected. The shallower one is the most relevant on an engineering perspective, the resulting approximate equation given by Hallermeier was:

$$d_c = 2.28H_{S12} - 68.5\left(\frac{H_{S12}^2}{gT_S^2}\right)$$

where, H_{s12} (also known as effective wave height H_e) is the non-breaking significant wave height exceeded only 12hr per year and T_s (or else T_e) the associated wave period.

In 1985 Birkemeier re-evaluated the Hallermeier's formula comparing it with high-quality field measurements and came out with a better approximation of the formula:

$$d_c = 1.75H_{S12} - 57.9\left(\frac{H_{S12}^2}{gT_S^2}\right)$$

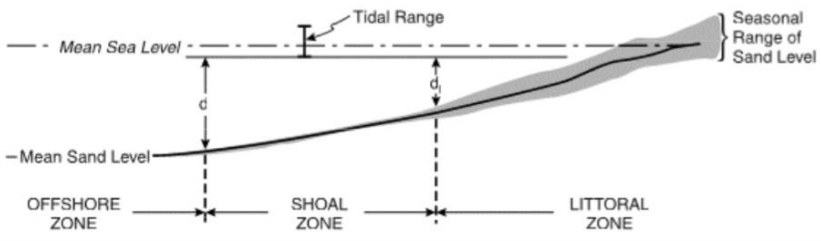

Figure 14: Sketch of the active closure depth. ***Font: CEM Part III chapter 3***

6. Computational models for static or dynamic response to storm effects

6.1 Static Models

It's already seen that any change in wave conditions or water level will result on a new profile equilibrium. Models for the calculation of the new profile may be basic static models or more complicated dynamic models, whether the sea conditions change on a slow or rapid way, respectively. The very first and best-known static model, relating shoreline retreat to an increase in local sea level, is the one proposed by Per Bruun in 1962. Bruun's rule is based on the exchange of sediment between the two profiles, and so requires the principle of mass conservation. The basis of the rule is the superposition of two shoreline responses within the closed area defined by the closure depth, stated as where significant sediment transport is performed in its entirety. First, the obvious retreat of shoreline due to sea rise, denoted as R_∞, which produces a positive sediment volume yield $\Delta V_+ = R_\infty(h_* + B)$, where h_* is the closure depth or depth of effective motion and B is the berm heigh. But there is also a volume of sand demand necessary to raise up the slope profile and maintain an equal equilibrium profile for the new water elevation. This required volume is expressed as $\Delta V_\infty = SL_*$, where S is the sea rise and L_* the active width of the active area. By superposition of both formulas and supposing that no sand mass is lost, Bruun proposed the following relationship: (note that the subscript ∞ indicates a static response)

$$R_\infty = S\frac{L_*}{h_*+B}$$

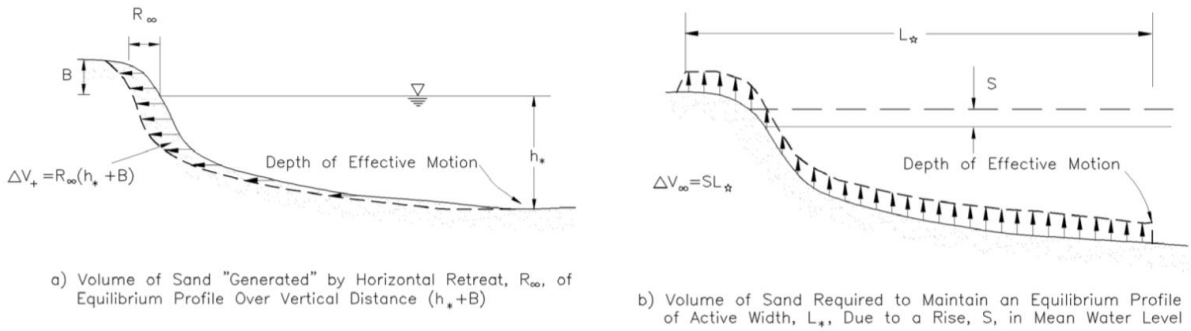

Figure 15: Components of sand volume balance due to sea level rise. ***Font: CEM Part III chapter 3***

The superposition effect slope results on a translation of the slope toward inland, with eroded sediment from the dry beach coast deposited on the end of the slope offshore, maintaining this way a net balance of sediment. The geometry of the new slope is shown on the following figure:

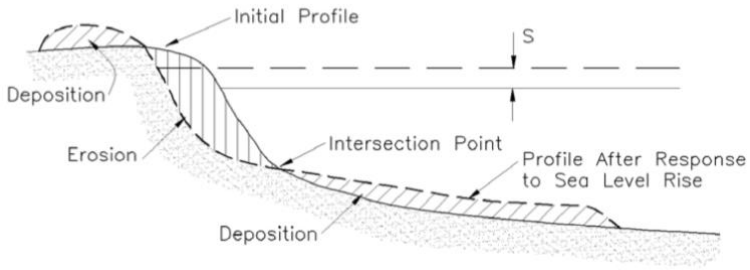

Figure 16: Brunn's Rule associated profile retreat *Font: CEM Part III chapter 3*

Although there have been several modifications and based on empirical applications to the Bruun's Rule, some aspects still have remained problematic due to the simplicity of the analysis and the supposition of net balance of sediment. Since the upper limit of the active profile is not clearly defined, it is difficult to find a realistic profile width L_*. Kriebel and Dean in 1993 improved Bruun's formula based on the studies on two profiles, one with a vertical face at the water line and with a sloping beach face.

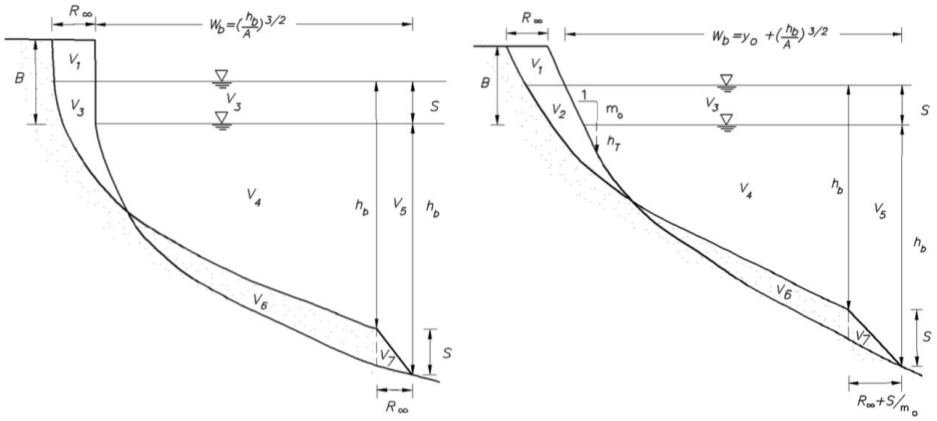

Figure 17: Profiles with vertical and sloping beach face considered by Kriebel and Dean (1993). *Font: CEM Part III chapter 3*

They proved that taking into account the small wedge-shaped area of sand volume offshore the breaking depth, better-quality expressions for the potential beach recession due to raised water levels could be established. Results for sloping beach face retreat of shoreline, R_∞, considering the slope of the beach profile at the waterline m_o are the following, vertical face profile is just a singular limiting case of the former one:

$$R_\infty = S\frac{W_b - \frac{h_b}{m_o}}{h_b + B - \frac{S}{2}}$$

$$W_b = y_o + \left(\frac{h_b}{A}\right)^{\frac{3}{2}}$$

where, W_b is the surf zone width calculated accounting a small offset of the shoreline between the sloping beach face and the imaginary or virtual origin of the equilibrium profile, detonated as $y_o = \frac{4A^3}{27m_o^3}$.

They also established the formula for the calculus of the volume eroded from the berm above the initial still-water level due to a storm surge level S, V_∞.

$$V_\infty = R_\infty B + \frac{S^2}{2m_o} - \frac{2}{5}\frac{S^{\frac{5}{2}}}{A^{\frac{3}{2}}}$$

Under more realistic situation and beach face slopes, the results of the potential berm recession either for Bruun's or Dean's solutions would give smaller estimates. That is due to the portion of the rise in water level accommodated by shifting up the shoreline on the sloping beach face, and so, less berm retreat is required. The overestimation erosion associated with these models fulfills a safety factor for any engineering purpose.

6.2 Dynamic Model

Dynamic computational models are distinguished from the former static models by considering for the transient natural adjustment of the profile. Basically these models are ruled by a continuity equation, such as the conservation equation, and a dynamic transport equation. The conservation equation balances the differences between incomes and outcomes from the region of study as predicted by transport equation.

For the numerical modeling, two representations of the sea bottom physical domain are considered. The first one considers finite increments of the distance *y* to draw infinitesimal rectangles of the profile. The independent variable is the distance *y* and the dependent variable is depth *h*, which varies with time. The second type differs on considering finite increments of the depth *h*, drawing horizontal rectangles. In this case, the dependent variable, varying with time, is the distance *y*. The first type is more advantageous than the latter, as it can represent bars with no difficulties.

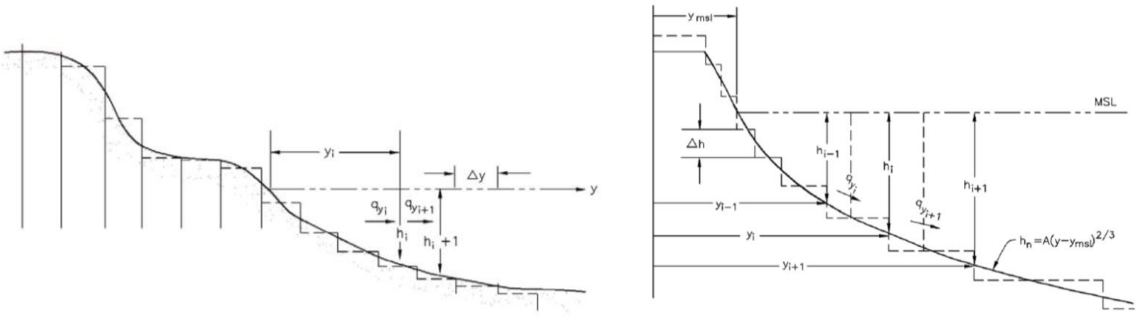

Figure 18: Types of grids for numerical modelling. ***Font: CEM Part III chapter 3***

The conservation equation for the first type, in which the independent variables are *y* and *t*, is the following:

$$\frac{\partial h}{\partial t} = \frac{\partial q_y}{\partial y}$$

If h and t are the independent variables, as in the second type, the conservation equation is:

$$\frac{\partial y(h)}{\partial t} = -\frac{\partial q_y}{\partial h}$$

where q_y is the sediment transport quantity. It is noted that for each depth value *h*, there is an associated distance value *y*.

Sediment transportation relationships vary from two categories, the *closed loop* that converge to a target profile and *open loop*, which is a more faithful processes since it depends on the detailed hydrodynamics properties. Kriebel and Dean in 1985 proposed one of the first closed loop transport relationships. They assumed a simple transport relationship, retracting that the equilibrium beach profile is consistent with uniform wave energy dissipation per unit water volume D_*, expressed as:

$$q_y = K'(D - D_*)$$

where the parameter *K'* is used to calibrate the model by associating the sediment transport rate to the excess energy dissipation. Note that in equilibrium, $D=D_*$.

Larson and Kraus in 1989 modified the transport relationship made by Kriebel and Dean to be consistent with a profile with beach face slope m_o:

$$q_y = K''(D - D_*) + \epsilon \frac{\partial h}{\partial y}$$

where ϵ is an additional model parameter. The parameter K'' differs from the former

one of the Kriebel and Dean's relationship since considers the additional gravitational effects by the slope term which moves sediments offshore.

The equilibrium energy dissipation per unit volume D_* is given by:

$$D_* = \frac{5}{24}\,\rho\, g^{\frac{3}{2}}\,\kappa^2\, A^{\frac{3}{2}}$$

where the equilibrium profile parameter A is determined rather from the sediment grain size or from the best-fit of the equilibrium profile equation $h = Ay^{2/3}$.

7. Nourishment profiles

The aim of beach nourishment is to create a wider beach by artificially increasing the quantity of sediment on a beach that has experienced sediment loss. Offshore sediment, obtained from dredging operations, is typically used since it has already been subjected to marine sorting instead of a more landward source. When nourishing beaches, it is important to consider the resultant dry beach width after profile equilibration, Δy. Generally the added sand is placed under slopes significantly steeper than the equilibrium one and over a period of several years the equilibrium process redistributes the fill sand across the active profile of to the depth of closure. The results will be a function of the compatibility of the filled sand, A_F, and the native sand, A_N. For equilibrium profiles, coarser sediments derive to steeper profiles than finer sediments, thus beach fills using coarser sand will need less sediment to offer the same equilibrium dry beach width than a filling of finer than the native sand.

Depending on the sand grain size respect to the original beach sand and on the volumes added, three different resulting profiles are expected, termed as *intersecting*, *nonintersecting* and *submerged*. Nonintersecting or submerged profiles always happen if the sediment grain size is finer or equal than the natural one, whereas intersecting profiles require coarser filled sand, although coarser sediments do not imply an intersecting profile, as the intersection may occur at a depth deeper than the depth of closure. Only effects of cross-shore equilibration will be considered, but it is important to be aware that in design of beach nourishment projects the additional effects of a more rapid spreading out of the added sand appears, due to long-shore sediment transport.

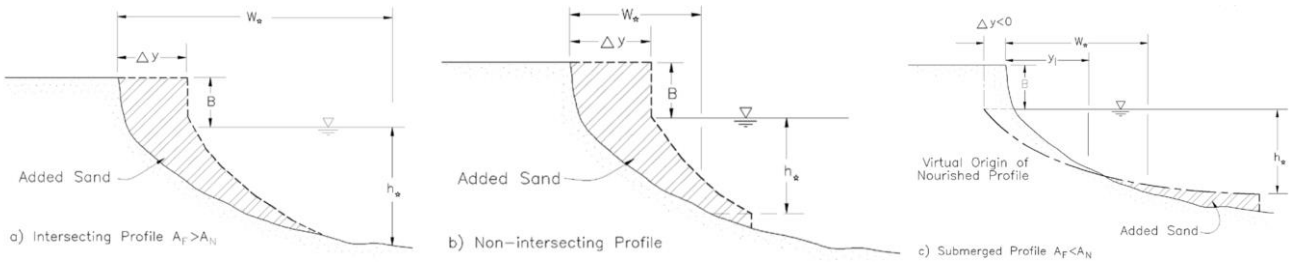

Figure 19: Representation of intersecting, non-intersecting and submerged profiles

To study the profile type occurrence the definition of the following nondimensional quantities is useful:

$$A' = \frac{A_F}{A_N} \qquad \Delta y' = \frac{\Delta y}{W_*} \qquad B' = \frac{B}{h_*} \qquad V' = \frac{V}{B \cdot W_*}$$

where, V is the added volume per unit beach length, B the berm height, h_* the depth to which the nourished profile will equilibrate, in general considered to be the closure depth, and W_* is a parameter based on the native sediment scale parameter A_N shown to be:

$$W_* = \left(\frac{h_*}{A_N}\right)^{\frac{3}{2}}$$

The non dimensional equilibrium dry beach width, $\Delta y'$, is a function of the other three non dimensional parameters:

$$\Delta y' = f(B', V', A')$$

The intersecting or nonintersecting profiles are conditioned by the following relationship:

$$\Delta y' + \left(\frac{1}{A'}\right)^{\frac{3}{2}} - 1 \begin{cases} < 0, intersecting\ profiles \\ > 0, non\ intersecting\ profiles \end{cases}$$

The critical volume of sand for intersecting and nonintersecting profiles is shown to be:

$$(V')_{c1} = \left(1 + \frac{3}{5B'}\right)\left[1 - \left(\frac{1}{A'}\right)^{\frac{3}{2}}\right],\ for\ A' > 1$$

$$(V')_{c2} = \frac{3}{5B'}\left(\frac{1}{A'}\right)^{\frac{3}{2}}\left(\frac{1}{A'} - 1\right),\ for\ A' < 1$$

For *A' < 1* the profiles will always be nonintersecting but it has to be noted that nonintersecting profiles may exist for *A' > 1*. If *A' > 1* and *V' > V'c1* the profile will be nonintersecting, whereas if the second inequality is not met, the profile is intersecting.

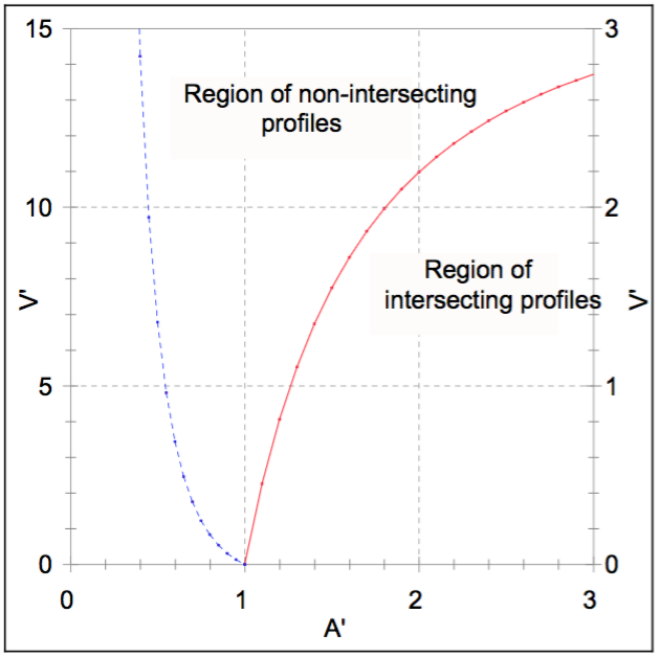

Figure 20: Results presented for B' = 0.25. ***Font: CEM Part III chapter 3.***

Finally, the nondimensional volumes required to yield an advancement $\Delta y'$ for intersecting, V'_1 and nonintersecting profiles, V'_2 are:

$$V'_1 = \Delta y' + \frac{3}{5B'} \frac{(\Delta y')^{\frac{5}{3}}}{\left[1 - \left(\frac{1}{A'}\right)^{\frac{3}{2}}\right]^{\frac{2}{3}}}$$

$$V'_2 = \Delta y' + \frac{3}{5B'} \left\{ \left[\Delta y' + \left(\frac{1}{A'}\right)^{\frac{3}{2}} \right]^{\frac{5}{3}} - \left(\frac{1}{A'}\right)^{\frac{3}{2}} \right\}$$

For submerged profiles those relations vary a little, since $\Delta y' < 0$ and $A' < 1$:

$$\frac{\Delta y}{y_I} = 1 - \left(\frac{1}{A'}\right)^{\frac{3}{2}}$$

And the nondimensional volume of sediment, V'_3, is expressed as:

$$V'_3 = \frac{3}{5B'}\left\{\left[\Delta y' + \left(\frac{1}{A'}\right)^{\frac{3}{2}}\right]^{\frac{5}{3}} + \frac{(-\Delta y')^{\frac{5}{3}}}{\left[\left(\frac{1}{A'}\right)^{\frac{3}{2}} - 1\right]^{\frac{2}{3}}} - \left(\frac{1}{A'}\right)^{\frac{3}{2}}\right\}$$

Alternatively to nourishment, it will be interesting to mention some hard structural or engineering options normally used to prevent and protect the shore from coastal erosion under big waves or notable long-shore sediment transport. It may be structures constructed on the beach or further offshore, which influence coastal processes and stop or reduce the rate of coastal erosion.

To trap long-shore sediment transport or control long-shore currents, groynes are used, consisting on a coastal structure constructed perpendicular to the coastline all along the shoreline, from the beach into the sea. They are easy to construct and from a variety of materials such as wood or rock, but it has the disadvantage of causing erosion downdrift, which requires regular maintenance. Otherwise, artificial headlands can be constructed, used to promote natural beaches. It is a relatively large structure but it is easy to build and needs little maintenance, although it has poor stability against large waves.

Figure 21: Groynes along the coastline. ***Font: http://www.stacey.peak-media.co.uk/EastonBavents/EastonCovehitheSep2009***

Constructed parallel to the coastline, in order to prevent cross-shore sediment transport, seawalls shelter the shore from wave action, improve slope stability and can also dissipate wave energy on sandy coasts. It should be constructed along the whole

coastline, or else erosion could occur on the adjacent coastline and it has to be noted that it creates wave reflections that promote sediment transport offshore.

Finally, really common to see, there is the option of constructing offshore breakwaters, consisting on a structure parallel to the shore, in the near-shore zone, that serves as a wave absorber. They reduce wave energy and its lee and create a salient behind the structure that influences long-shore sediment transport. Unfortunately these structures are vulnerable to strong wave action for what they need a special design, making them huge buildings relatively difficult to build.

Figure 22: Offshore Breakwaters. ***Font: http://the-earth-story.com/post/101203549140/breakwaters-and-jetties-in-an-effort-to-reduce***

PRACTICAL PART

8. Objectives

The aim of this project is to analyze the capacity of waves to induce an onshore/offshore sediment transport along the Catalan coast. The results will serve to evaluate the capacity of beaches to recover the original shape after the pass of an extreme event.

After studying the basic beach morphological properties, such as bar generation or accretive or erosive profiles, and the forces or actions acting within the near-shore, 5 different parameters were chosen in order to estimate the landward or seaward sediment transport. These parameterizations are used by coastal engineers to estimate seasonal changes in beach morphology, especially when developing projects related to beach conservation, restoration or artificial beach nourishment.

To parameterize beach erosion or accretion conditions, we need a certain processed data. We will need to gather a set of characteristics of the incident waves, such as the wave high H_0, its period T and wavelength $L_{0,}$ and the fall velocity of the sediment particle, w. For this last one, we will need a register of the morphology of the Catalan beaches, including the sediment particle size d_{50} and the beach slope, expressed as $tan\beta$.

From there, it will be possible to compare the behaviors of the different predictive formulations and how they relate, and predict the evolutionary state of each of the beaches along the Catalan coast, in a qualitative way or trying to estimate the amounts. Finally to conclude, we will be able to discuss the results and suggest solutions according to the ones already seen in the theoretical part, such as beach nourishment or external structures.

9. Data

The first set of data, corresponding to the morphological properties along the Catalan coast, was obtained from the Institut Cartogràfic I Geològic de Catalunya (ICGC). The information consists on empirical measured data of each of the 331 existing beaches, some divided by north or south regions increasing it to 390, regarding sediment grain characteristics (size and color) and beach profile characteristics.

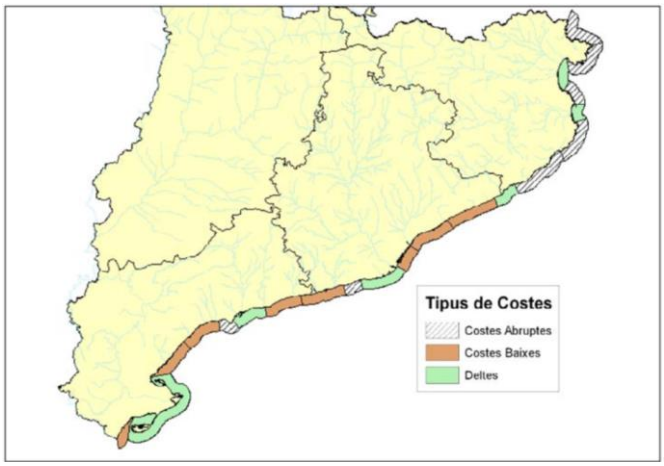

Figure 23: Types of coast of Catalonia, grey for abrupt coasts, green for delta coasts and orange for small steep coasts. *Font: ICGC, LLibre verd de l'Estat de la zona costanera de Catalunya, 2010*

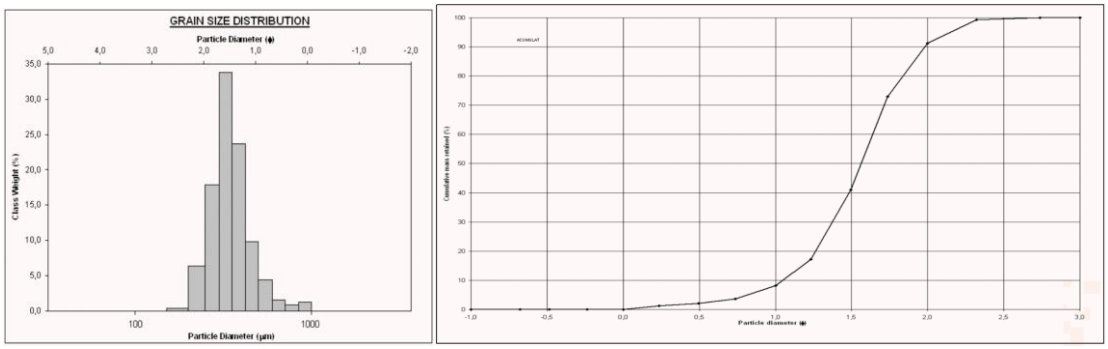

Figure 24: Sediment granulometric description of *La Fosca* beach

Previously, a zonification and division of the Catalan coast was determined by identifying coast cells. These cells are defined as independent stretches of coastline from the point of view of coastal dynamics. The division doesn't necessary mean having no connection to the adjacent coast, but head-to-head coasts can be connected by means of boundary conditions. For each of these sectors, the coast dynamics is characterized, determining the evolutionary state function, which is categorized at long term.

The 390 beaches or beach regions of the Catalan coast, 159 in the province of

Tarragona, 109 in Barcelona and 122 in Girona, have been regrouped in 22 different coast cells. From south to north, the first 6 cells correspond to the 127 beaches of Tarragona, the coast of Barcelona is represented from the 7th cell to the 15th and the last 7 coastal stretches, from the 16th to the 22nd, define the 104 beaches of Girona.

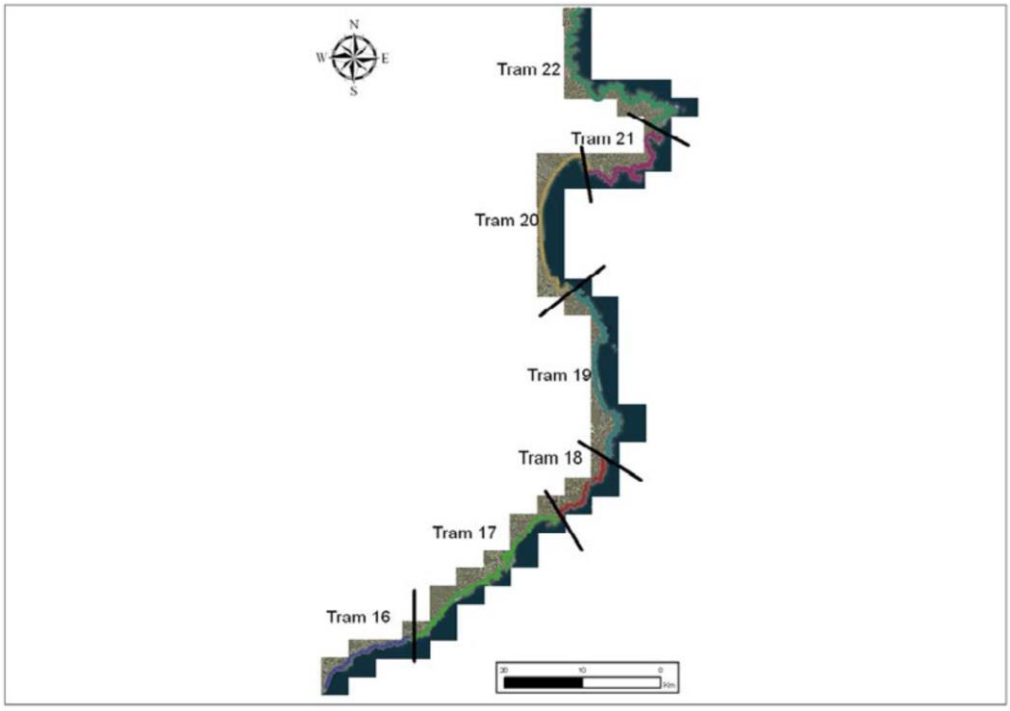

Figure 25: Coastal cells defined for Girona's coast. ***Font: ICGC, LLibre verd de l'Estat de la zona costanera de Catalunya, 2010***

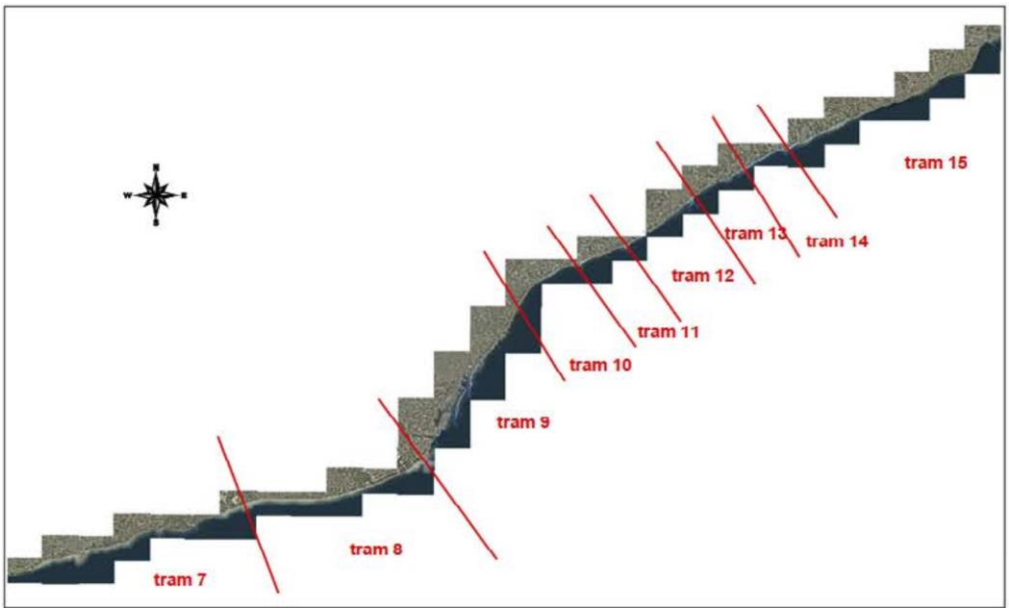

Figure 26: Coastal cells defined for Barcelona's coast. ***Font: ICGC, LLibre verd de l'Estat de la zona costanera de Catalunya, 2010***

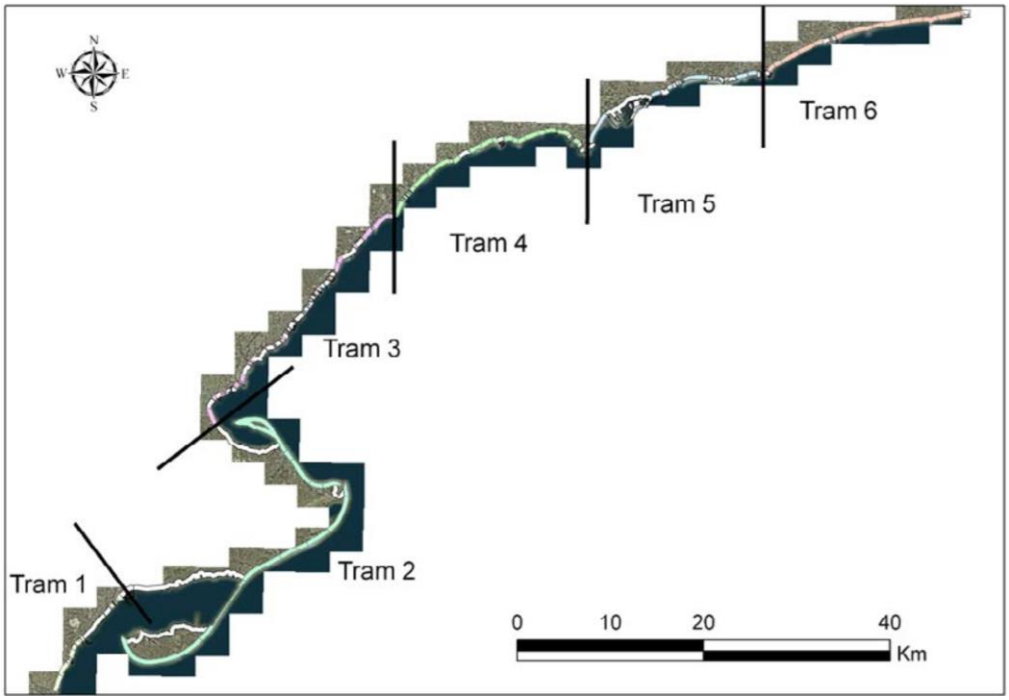

Figure 27: Coastal cells defined for Tarragona's coast. ***Font: ICGC, LLibre verd de l'Estat de la zona costanera de Catalunya, 2010***

Tram	Id-sig	LIM	CODE	d_{50} (mm)	TANβ	mean	σ (mm)
7	1	01 P. de les Salines	GAVG001	0,144	0,08	1,547	0,03519
7	2	02 P.de la Mota de Sant Pere	GAVG002	0,1456	0,08	1,572	0,03913
7	3	03 P.Llarga de Cubelles	GAVG003	0,1952	0,08	0,206	0,06326
7	4	04 P. Ibersol	GAVG004	0,1858	0,08	0,207	0,0945
7	5 sur	05_P.Llarga de Vilanova Sur	GAVG005	0,1755	0,08	0,183	0,04708
7	5 norte	05_P.Llarga de Vilanova Nord	GAVG005	0,3885	0,08	0,421	0,1783
7	6	06_P. de Sant Gervasi	GAVG006	0,1838	0,08	0,193	0,04947
7	7	07_P.de Adarro	GAVG007	0,1807	0,08	0,1888	0,0455
7	8	08_P.de Ribes Roger	GAVG008	0,1488	0,08	0,16	0,03498
7	9	09_P. del Far de sant Cristofol	GAVG009	0,1584	0,08	0,1748	0,05395

Table 3: Example of data obtained from the ICGC for each of the Catalan beaches. ***Font: ICGC, LLibre verd de l'Estat de la zona costanera de Catalunya, 2010***

A set of characteristics of the incident waves is also needed and can be found at the Organismo Publico Puertos del Estado, Ministerio de Fomento. The information comes from measured and modeled data. Measured data is derived from buoys (REDEXT, REDCOS) and modeled data (SIMAR) is obtained both from reanalysis and operational forecasting systems.

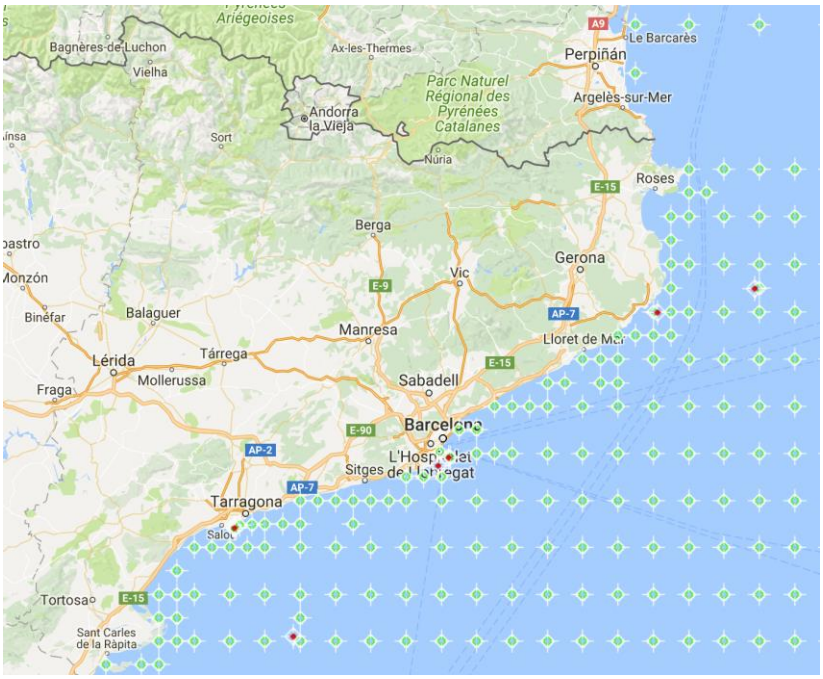

Figure 28: SIMAR points and buoys along the Catalan coast. ***Font: Organismo Publico Puertos del Estado, Ministerio de Fomento***

Each SIMAR point gives us the every hour registration, from the January 4th 1958 to the 20th of July 2016, of the modeled spectral wave height H_{m0} in meters, its peak spectral period T_p in seconds, its middle spectral moment period 0 and 2 T_{m02} in seconds and the mean wave direction *DirM*, equal to 0 for North direction and 90 for East. It also provides various swell wave heights, periods and directions estimations and the average wind speed and its direction. Buoys give measured scalar data and directional data of the waves calculated over periods of 26 min, as well as oceanographic and meteorological data calculated over periods of 10 min.

From all the offered points provided, we are interested in getting diverse data from deep-sea waves corresponding to the different independent coastal cell areas already defined. In order to obtain more centralized data, we have chosen 8 SIMAR points spread throughout the Catalan coast to work in smaller data fields, apart from the measured data obtained from the 4 Catalan buoys.

The 8 chosen SIMAR points and their respective cells of work are shown in the table below, from South to North:

SIMAR POINT	COASTAL CELL
2098128	1 and 2
2098130	3 and 4
2104132	5, 6 and 7
2114134	8, 9, 10 and 11
2118136	12, 13, 14, 15 and 16
2124140	17 and 18
2126146	19 and 20
2128148	21 and 22

Table 4: SIMAR points and their respective cells of work. ***Font: Organismo Publico Puertos del Estado, Ministerio de Fomento***

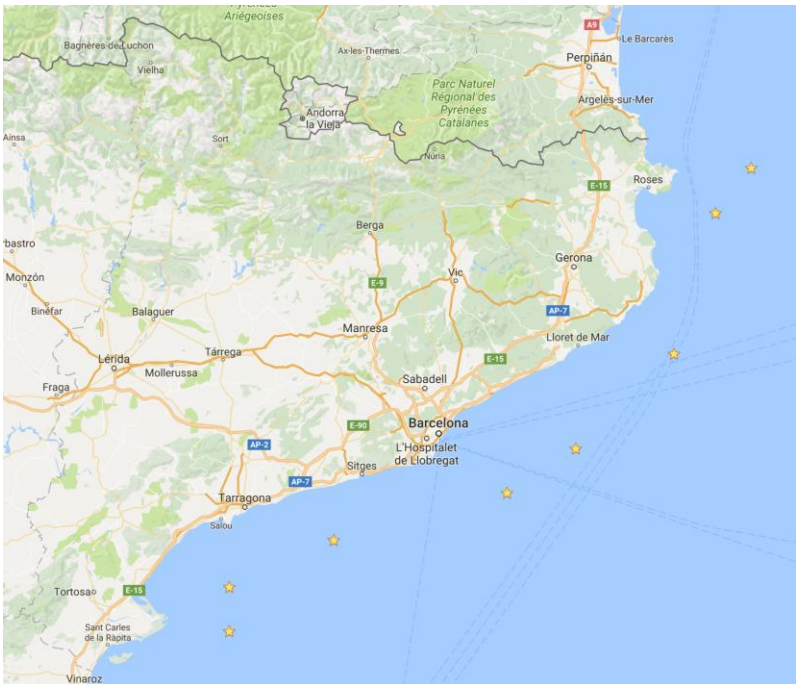

Figure 29: Map of the 8 chosen SIMAR points. ***Font: www.maps.google.com***

10. Data Analysis

The total data of incident waves is very extensive and thus it might be useful to treat all values carefully and understand them before starting any calculation. For it, the almost 511.000 hourly values of the wave height H_{m0}, period T_p, wavelength L_0 and its direction, have been examined and discretely separated per seasons, differentiating between winter, from September to May, and summer, from June to August, or divided taking into consideration the average direction of provenance of the waves, setting a North, East, South and West directions with a 45º angle wide. The idea is to determine any behavior pattern along the time history data that could help us understand better the final results.

10.1 Seasonal Analysis

Winter has always been determined to be the highest energy season, comprising the highest and longest waves and resulting on a winter or erosive profile, characterized by a flatter foreshore and the existence of an offshore bar due to the accumulation of eroded sediment at the breaking zone. On the other hand, summer is the mild energy season, with lower waves and thus leading to a normal or accretive profile, with absence of a bar but the appearance of a berm instead.

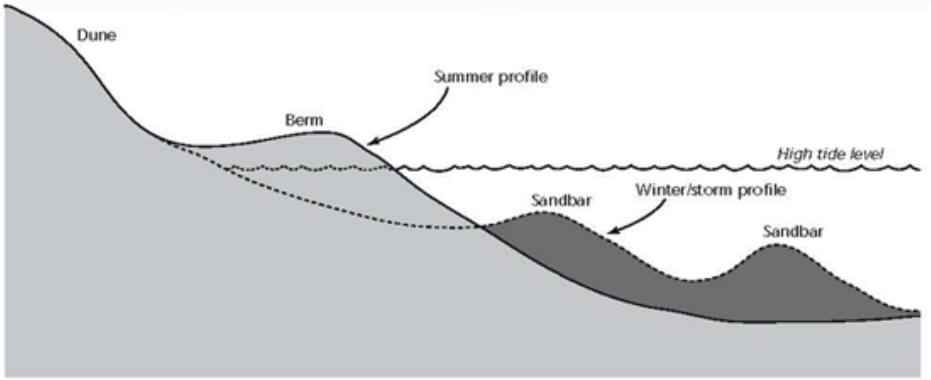

Figure 30: Typical summer and winter beach and dune profiles. ***Font:*** **O'Connell, J., 2000. WHOI Sea Grant Program, Marine Extension Bulletin, "Beach and Dune Profiles: An Educational Tool for Observing and Comparing Dynamic Coastal Environments"**

The two seasons, divided between September-May and June-August, comprises the 74,8% of the values and 25,2%, respectively. For a clearer representation of the difference between summer and winter, we have analyzed the distribution of waves with respect to their different wave heights, from those waves lower than 0,5 meters, to the highest ones over 2 meters, with intervals of 0,5 meters.

The wave distribution of the 2 main seasons, for SIMAR 2098130 located in front of the Tarragona's coast and the northernmost point SIMAR 2128148, located in front of the *Cap de Creus*, is represented below:

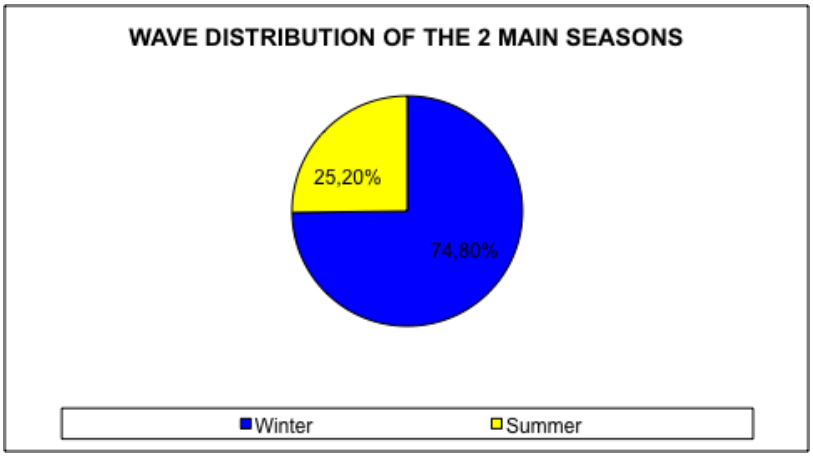

Figure 31: Wave data distribution over winter and summer seasons

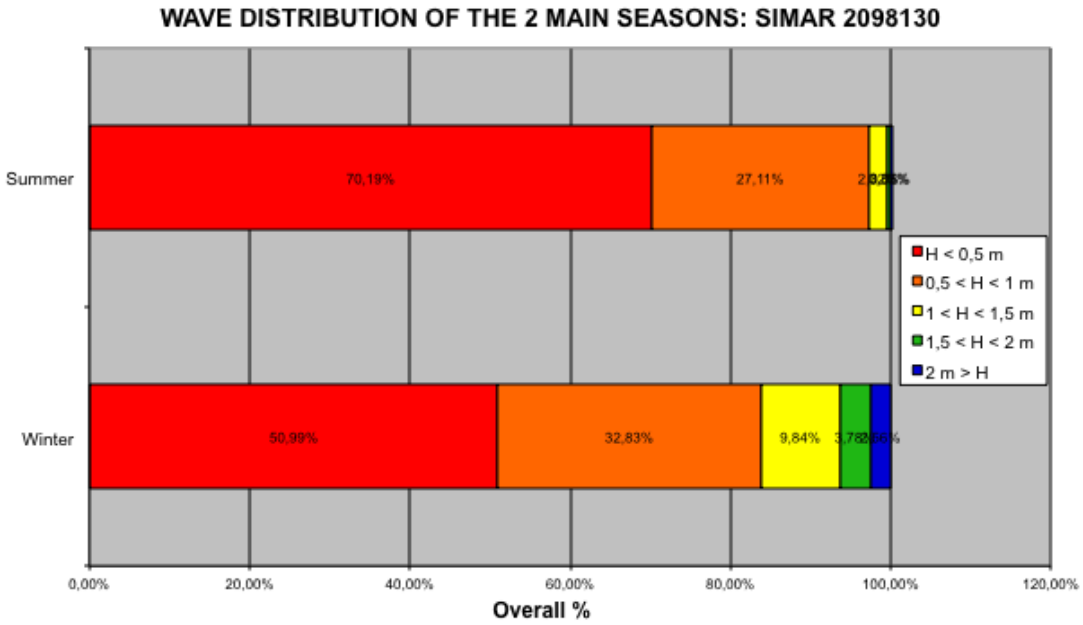

Figure 32: Wave height distribution throughout winter and summer seasons

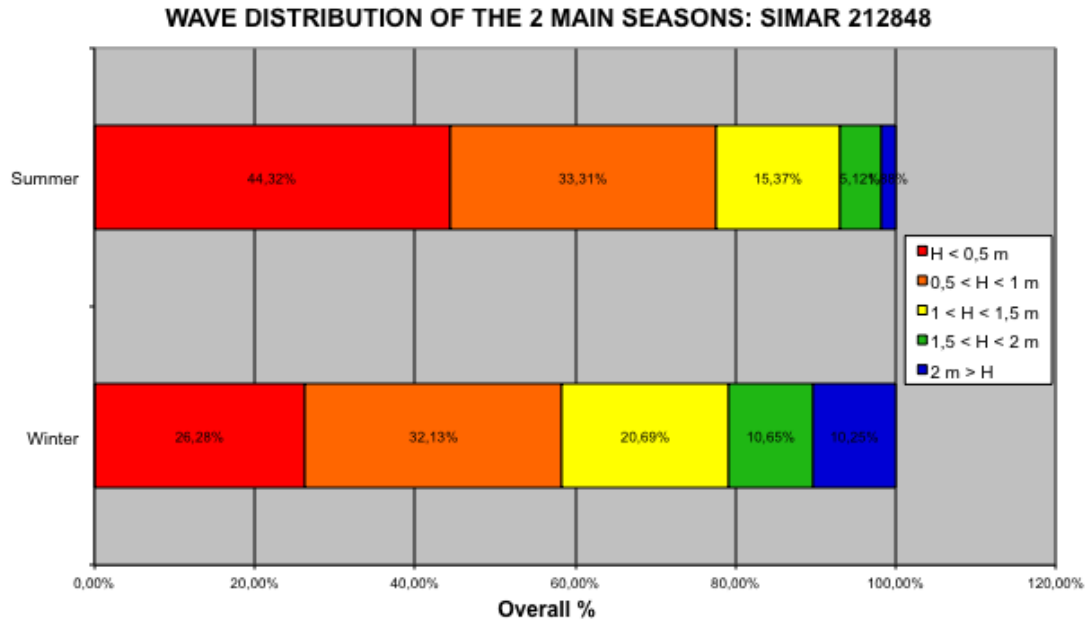

Figure 33: Wave height distribution throughout winter and summer seasons

Although this is just the representation of 2 of the 8 SIMAR points, the rest are found in the ANNEX, it is representatively enough to determine the seasonal pattern, as well as the coastal location pattern. As it was expected, summer, the mild energy season, gathers a lot of small waves and for all SIMAR points, waves below 1 meter height represent at least the 80% of the total summer wave height values. As for winter, small waves, lower than 1 meter, still are the majority but the percentage of the rest of the height intervals increase, in favor of a notorious reduction of the H<0,5m interval.

It is also clearly evidenced that as long as we go north, the wave distribution varies a lot, leading to higher values. Therefore, up in the north the number of low waves is decreased and the appearance of waves higher than 1,5 meters or even 2 meters is more common. These small conclusions are in accordance with our knowledge of the Catalan coast, since the north always has been characterized to be more violent, because of the constant south east wind and *Tramuntana* that it receives from the *Gulf of Lion*.

10.2 Directional Analysis

The same reasoning as before can be extracted for analysis of directional data. It is very illustrative to focus on the percentage of waves coming from the 4 main

directions. In fact, the 5 southern SIMAR points present a very dominant direction with more than 50% of the values coming from East. It is well known that the east of the Iberian Peninsula is hit by wind coming from the Mediterranean sea, therefore those results are the ones expected. Surprisingly, the point close to the south of Costa Brava has a North dominant direction of waves, and the two northernmost points have a very clear South direction. This may be explained by the proximity of the *Gulf of Lion*, redirecting the wind to north and south of the *Cap de Creus*.

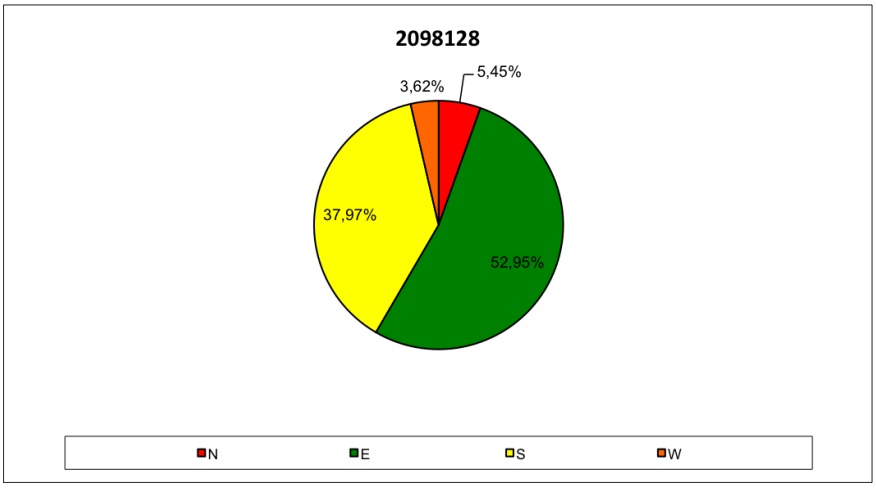

Figure 34: Directional wave distribution for SIMAR 2098128, located in front of the *Delta de l'Ebre*. Representative case of an East dominant direction of provenance waves

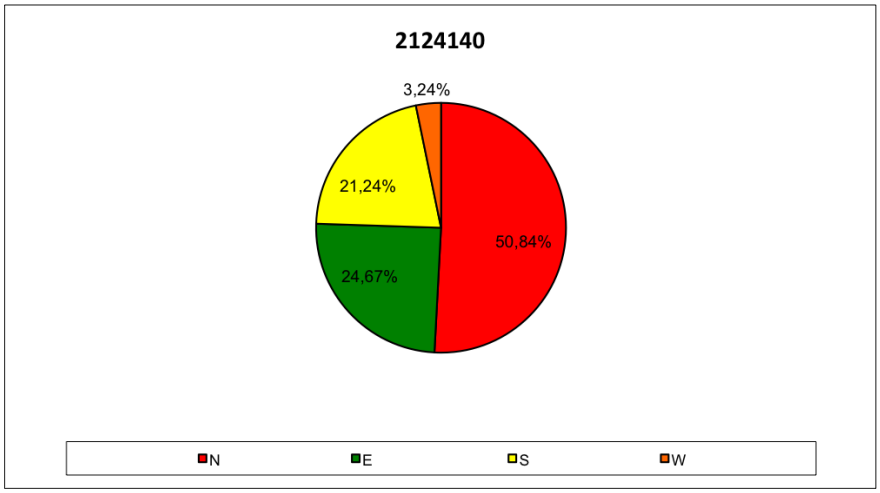

Figure 35: Directional wave distribution for SIMAR 2124140, located in front of the *South Costa Brava*, *Baix Emporda* and *La Selva* coasts. Unique case of a West dominant direction of provenance waves

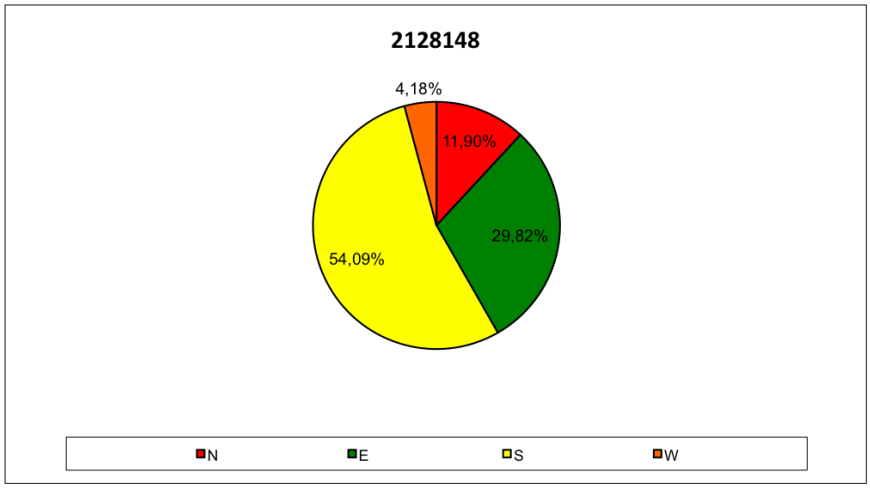

Figure 36: Directional wave distribution for SIMAR 2128148, northernmost point located in front of the *Cap de Creus*. Representative case of a South dominant direction of provenance waves

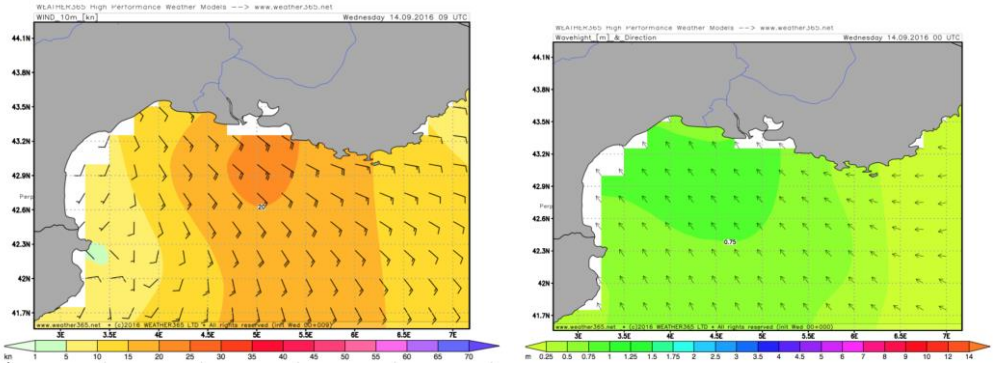

Figure 37: Typical configuration of wind directions and wind speed on the left, and wave heights and wave directions on the right. *Font: https://www.weather365.net*

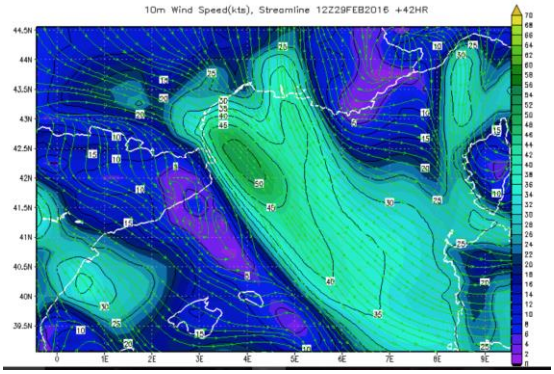

Figure 38: Representative scenario of wind speed of the North-East Mediterranean Sea. *Font: https://www.weather365.net*

Although it might not be the main direction or the most common, for all SIMAR points of study with just one exception, the East direction is the one that brings together the highest percentage of high waves, grouping waves higher than 1 meter. This means that despite much of the time the waves come from a certain direction, those waves tend to be low, and the direction with more energy, which brings along

bigger waves, comes from the East. And so, the 2 northernmost SIMAR points, which had the south direction as their main direction, present the following wave distribution:

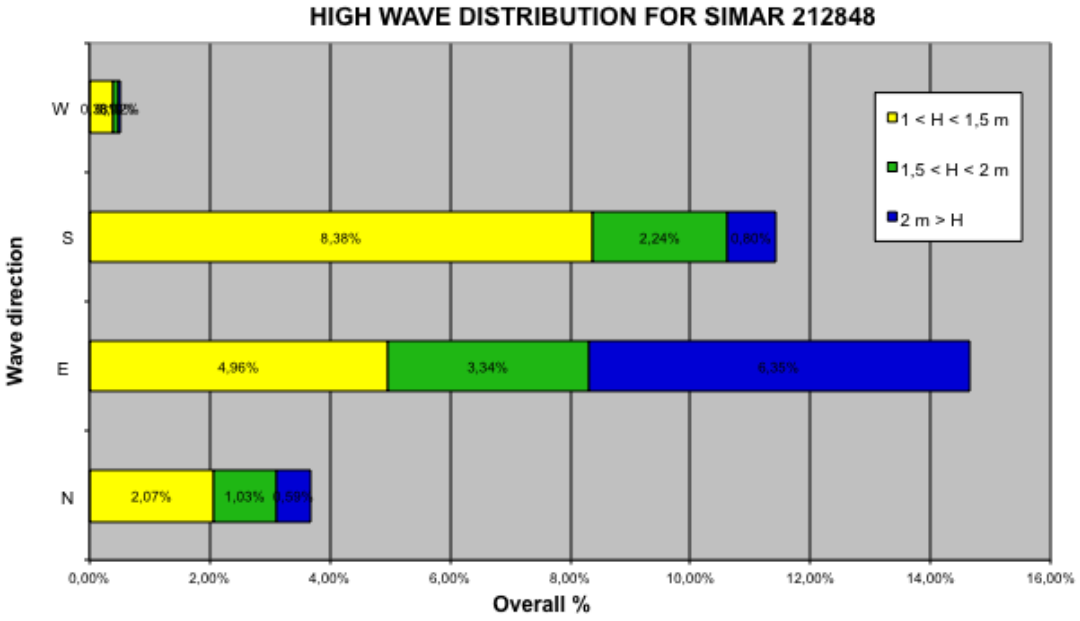

Figure 39: Directional distribution of waves higher than 1 meter, classified per heights, for SIMAR 212848, located in front of the *Cap de Creus*

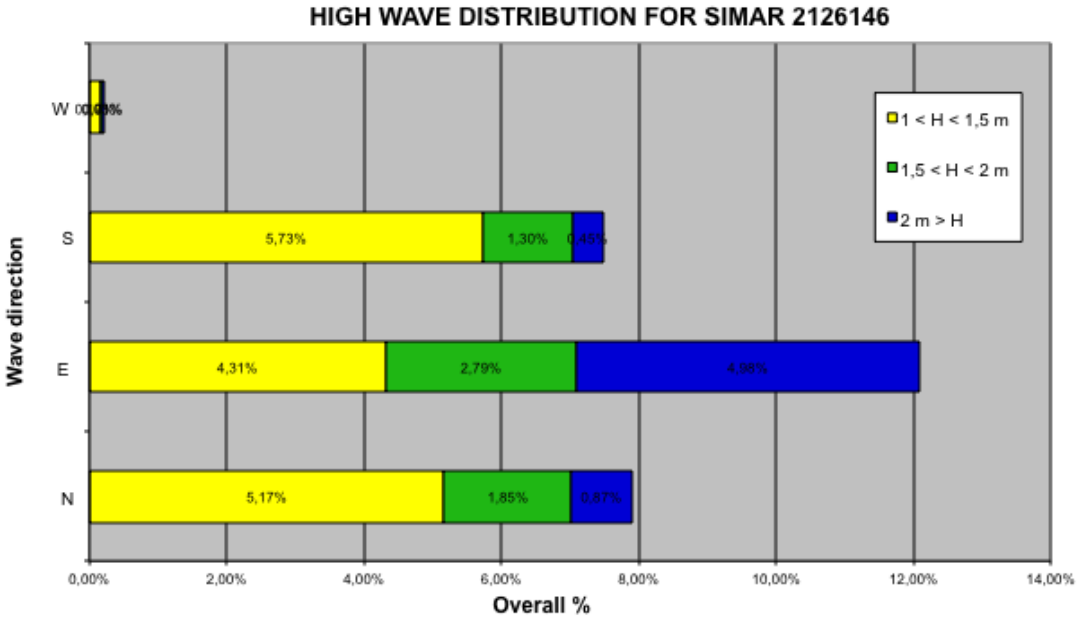

Figure 40: Directional distribution of waves higher than 1 meter, classified per heights, for SIMAR 2126146, located in front of the *Gulf of Roses*

The first 5 points, considering from south to north, already had the East as main direction and thus it has sense to think that their wave distribution gathers the most number of highest waves throughout the East direction.

The exception we talked about is the SIMAR 2124140 point, located close to the south of Costa Brava. As we have previously seen, it was the only point with a North main direction, and still when you look at the wave distribution for high waves, it keeps the direction North as the one assembling the peak waves. Although it is important to note that the East direction also gains relevance, since for waves above 2 meters it has practically the same quantity of waves as in the north wave direction, as we can see below:

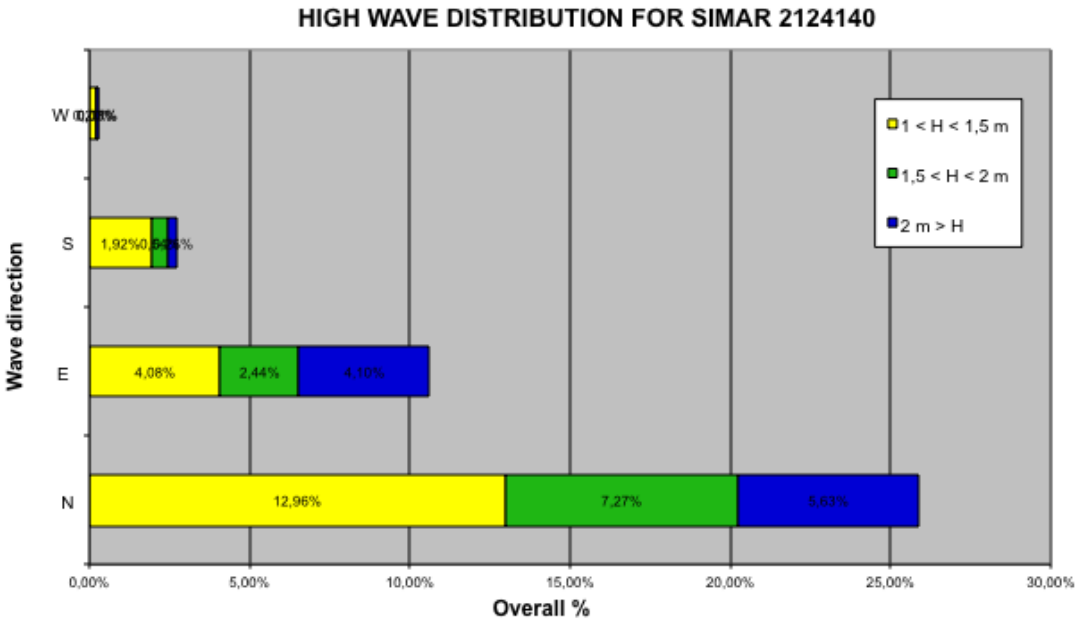

Figure 41: Directional distribution of waves higher than 1 meter, classified per heights, for SIMAR 2124140, located in front of the *South Costa Brava*, *Baix Emporda* and *La Selva* coasts

In order to see more clearly the seasonal or directional patterns, we can also plot the wave height and wavelength for all different data subgroups. Bellow, the representation of the mean wave height H_0 and the mean wavelength L_0, as well as their variation coefficient, let us compare the differences between seasons or directions for all the eight SIMAR points (1 to 8, from South to North):

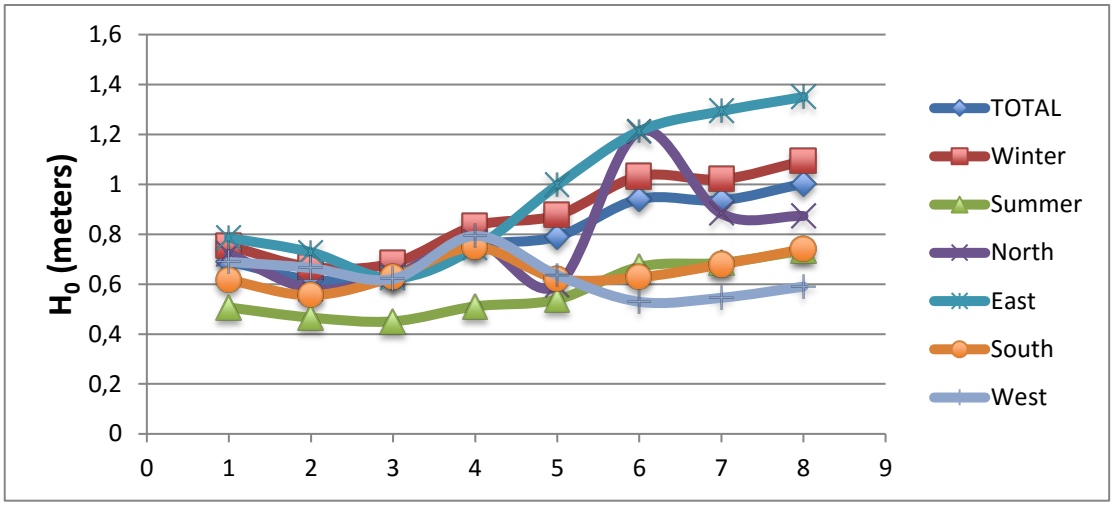

Figure 42: General, seasonal and directional mean wave height H_0 for every SIMAR point of study.

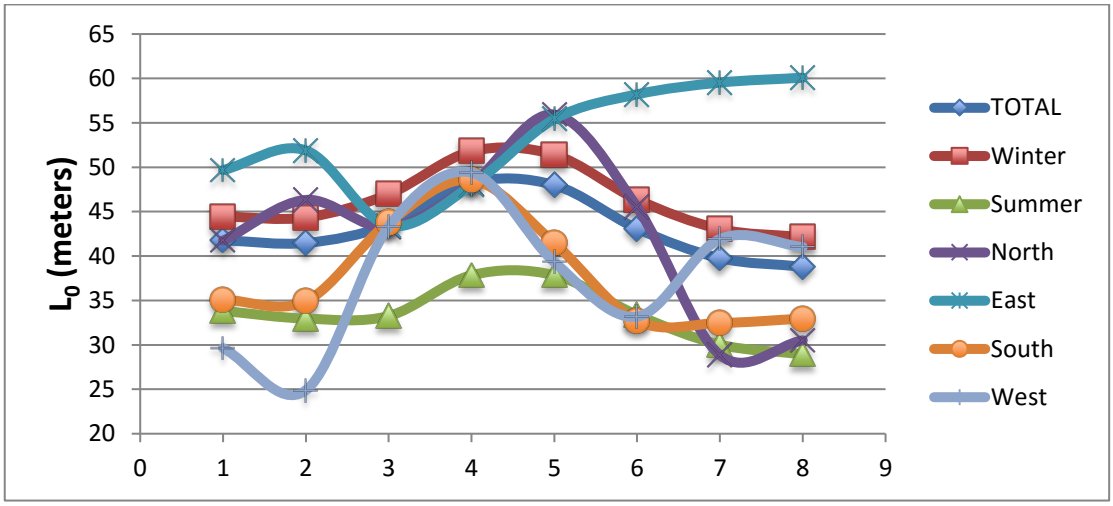

Figure 43: General, seasonal and directional mean wavelength L_0 for every SIMAR point of study

	Wave height H_0 Coefficient of Variation						
	TOTAL	**Winter**	**Summer**	**North**	**East**	**South**	**West**
1	0,749	0,748	0,546	0,728	0,762	0,716	0,540
2	0,755	0,761	0,538	0,732	0,758	0,725	0,577
3	0,759	0,752	0,573	0,738	0,762	0,756	0,763
4	0,774	0,751	0,624	0,741	0,762	0,790	0,796
5	0,772	0,749	0,639	0,753	0,822	0,683	0,699
6	0,761	0,740	0,675	0,643	0,810	0,666	0,623
7	0,778	0,765	0,675	0,648	0,802	0,610	0,646
8	0,755	0,738	0,677	0,721	0,795	0,619	0,673

Table 5: General, seasonal and directional wave height Variation Coefficient for every SIMAR point (from 1 to 8, South to North)

From this new point of view comparing the mean values, the earlier findings and conclusions are checked. It is important, however, to make a small point to variation coefficient, since their values are dangerously high, meaning these average values are not representatively enough of the totality of the data thus, it will not be appropriate

to work with, although it allows us to see on a broadly way the basic differences for every set of data.

It is very visual the difference of winter and summer values respect to the total, with the expected proportionally higher values for winter and lower values for the mild energy season.

Respect to the 4 different main directions, North, East, South and West, we can clearly see that the East direction comprises the highest values for every SIMAR point, regardless of their main direction throughout the whole data. It is also very remarkable the exception of the 6th SIMAR point, consisting on SIMAR 2124140, where as has already been discussed, the North direction is the main one and still is the direction that covers the highest values, but the East direction, although having less representative values, remains to be the direction that marks the most energy, so its average value of wave heights is very similar to the north.

10.3 Trends and Behavior Patterns Analysis

The analysis of the total set of data, or the seasonal data, in search of cyclical behaviors, behavior patterns or trends, can be also very important. Below we can see the representation of the last 2 years of wave height data for SIMAR 2124140, starting the 20th of July 2014 to the 20th of July 2016. The plot shows two clear high waves frequency zones corresponding to the winter periods, the latter being slightly milder:

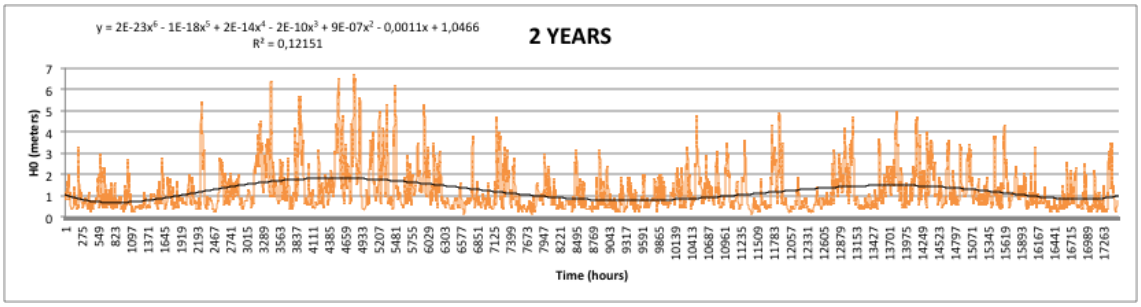

Figure 44: Representation of the two last years of wave heights H_0 for SIMAR 2124140 and its polynomial regression trend

The seasonal behavior can be summarized in a polynomial trend line of sixth grade. As was predictable, the maximums of this regression line define the winter season and thus represent a high-energy period, while the minimums and low areas represent the summer mild energy season.

We also wanted to analyze a little bit more in detail the possible trends within the same season, examining winter and summer separately. For it, we represented the wave height throughout a whole winter or summer and tried to find any cyclic pattern:

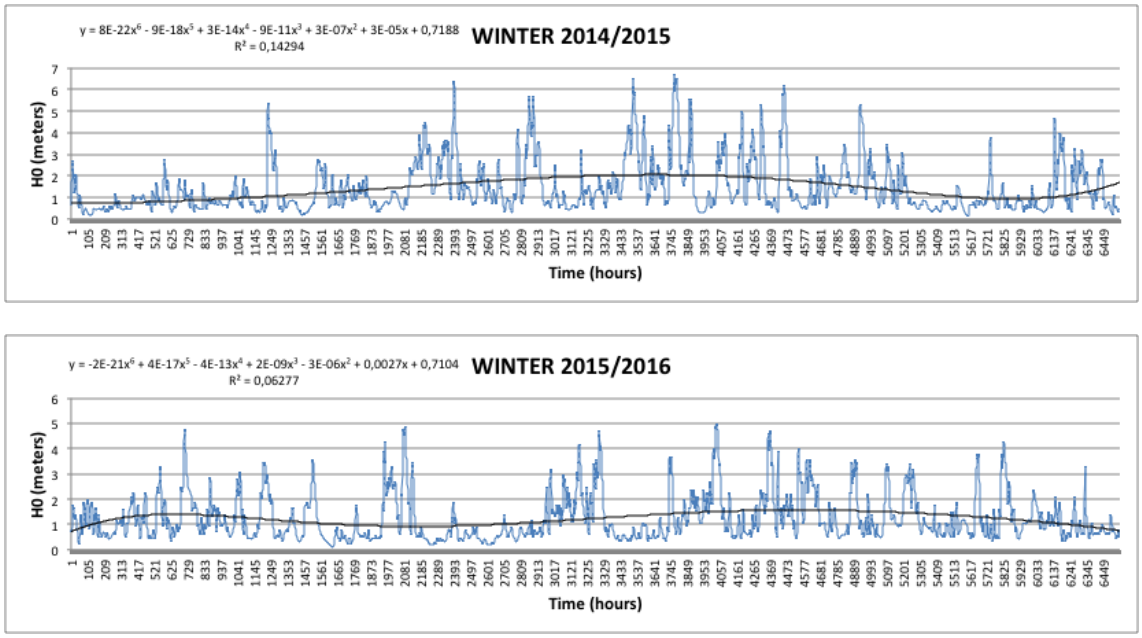

Figure 45: Representation of the two last winters (from September to May) of wave heights H_0 for SIMAR 2124140 and its polynomial regression trend

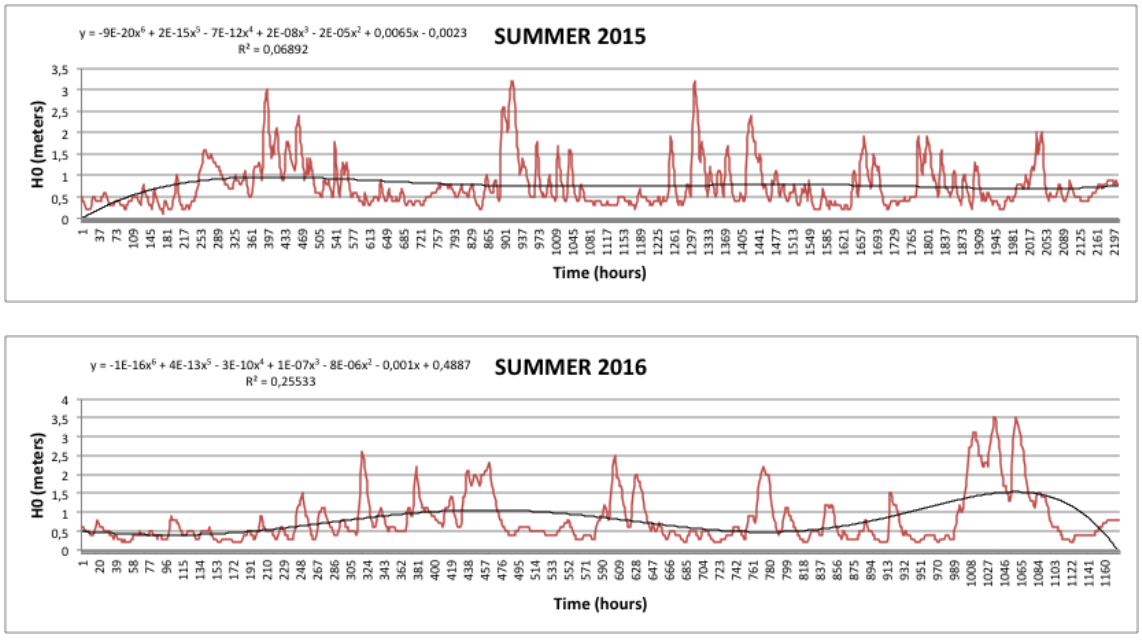

Figure 46: Representation of the two last summers (June to August, and June to the 20th of July) of wave heights H_0 for SIMAR 2124140 and its polynomial regression trend

However, it is difficult to find a line of very a definite trend within each season, being only able to see some ups and downs throughout the duration of the season,

more common in winter, defining different windstorms or precipitation periods but without a defined established pattern.

Anyway, the difference between summer and winter plots is remarkable. The lower values of wave heights, which are the more common data along the season, oscillate the 0,5 meters in summer, while in the winter the values range is close to 1 meter height. In addition, the difference between greatest peak values when there is an energetic stormy period for each season is also considerable, reaching between two and three meters height in summer and 4 to 5 meters in winter.

Finally, to study any long-term behavior pattern, we opted to apply a Fast Fourier Transform to the original data function in the time domain, obtaining a representation in the frequency domain. To do it, we required the use of the DEGTRA program, provided by the *Instituto de Ingeniería UNAM*, and we got the following results, equal for every SIMAR point just varying the Fourier Amplitude, being it higher for the northern and most energetic located points:

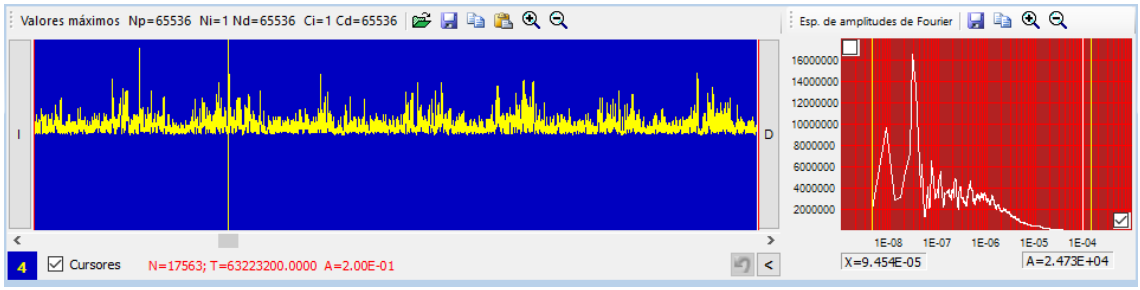

Figure 47: DEGTRA plots for the Fourier Spectra and the first 65536 values of wave height data, from January 1958 to July 1965, for SIMAR 2098128 located in front of the *Delta de l'Ebre*

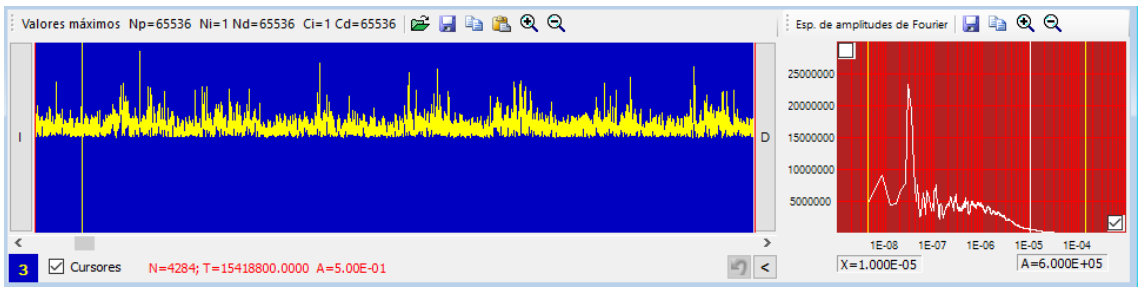

Figure 48: DEGTRA plots for the Fourier Spectra and the first 65536 values of wave height data, from January 1958 to July 1965, for SIMAR 2098128, northernmost point located in front of the *Cap de Creus*

DEGTRA is a program designed by the *Instituto de Ingeniería UNA of Mexico* and applied for engineering seismology to study seismic processes that last for dozens of seconds, therefore the only inconvenience of the program is that it proceeds to do the Fourier transform with a maximum of 65536 values, which corresponds to the 16th power of 2. As a consequence, our analysis of the long-term behavior patterns is reduced from the almost 58 years of data we have got to approximately 7 and a half years.

The lower frequencies of the Fourier spectra are related to long-term processes, while the higher frequencies, where the amplitude is decreased to 0, represent the short-term patterns. The peaks of amplitude configure the fundamental frequencies. Thus, the well-defined maximum peak located at low values of frequency determines the fundamental frequency for long-term behavior pattern, of the 7 and a half years of study.

This fundamental low frequency has a value of 2,97*10^-8 Hz. Knowing that Hz=1/seconds we can turn it to days or years by a simple transformation:

$$\frac{\mathbf{1}}{\mathbf{2,98 * 10^{-8} Hz}} = \mathbf{33670033,67\ s = 9352,78\ h = 389,69\ days} = \mathbf{1,068\ years}$$

This result means that approximately every year there is a repetition of behaviors, which can be easily related to yearly process of high and mild energy defined by winter and summer. Since our data was reduced to only 7 years, this is the longest long-term behavior pattern that we are able to find. We can perfectly see this yearly behavior on the 7 years data plot on the left of the Fourier spectra, as we can observe 7 blocks of high wave heights and 7 groups of low wave height values.

On the other hand, for high frequencies there is not a defined peak, nevertheless we can assume an average frequency value for the fundamental high frequency and try to identify a short-term behavior pattern. The fundamental high frequency value has been chosen approximately between 4,2*10^-7 and 4,32*10^-7 Hz, which transformed to days represent a cyclic pattern of 27,56 days to 26,79 days. These results can be directly related to the tides and the orbital period of revolution of the moon around the earth which is 27,32 days, also known as sidereal period or sidereal month.

Regarding the total set of data, it would be interesting to find a really long-term behavior pattern, which could be related to cyclic weather phenomenons such as the North Atlantic Oscillation or the still poorly known phenomenon of La Niña or El Niño.

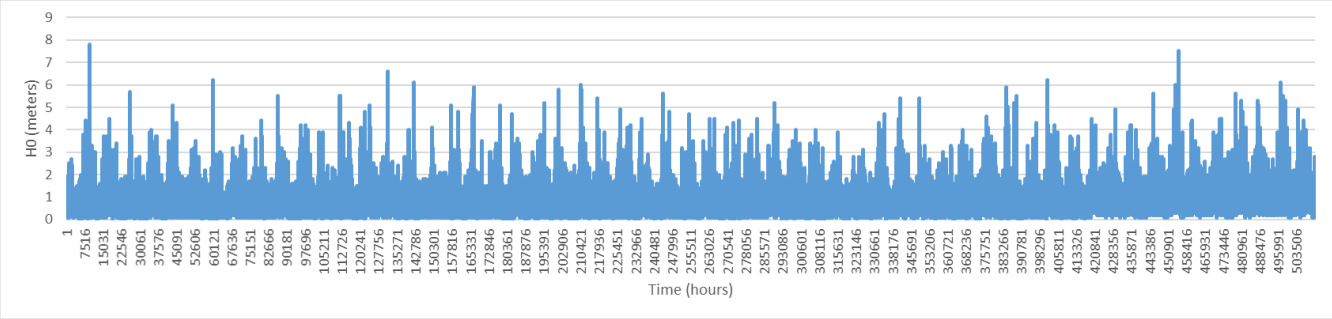

Figure 49: Representation of the whole set of wave heights H_0 data, from January 4th of 1958 until July 20th of 2016, for SIMAR 2118136

Unfortunately, it is very difficult to find any trend line sufficiently precise or any behavior pattern recognizable enough. This could probably be because of a lack of information or very limited and reduced set of data.

11. Results Analysis

This section is meant to comment on the main highlights and observations among the results. The objective is to compare global results given by the totality of the data set and the outcomes that are provided by reduced data, focusing on seasonal or directional analysis.

11.1 Pre-analysis and Overview

Before any operations are calculated and any results are given, we have to simplify the total set of data, basically wave height H_0, period T and wavelength L_0, and calculate the fall velocity w_f for each grain size, in order to be able to apply the different beach profile parameters.

11.1.1 Generic Unique Values for H_0, T and L_0

The problem that arises now is how to define generally, and in a unique value, the

every hour incident wave variables of the data. It may be interesting to define a wave height (within the set of N waves) in terms of probability, in example, the existing probability that a certain value of wave height *H* is exceeded within the set registered.

In 1952, Longuet-Higgins already made the assumption that waves are a random process and he defined that wave heights can be explained through a Gaussian distribution, demonstrating that a function of Rayleigh is the best representation of the progression.

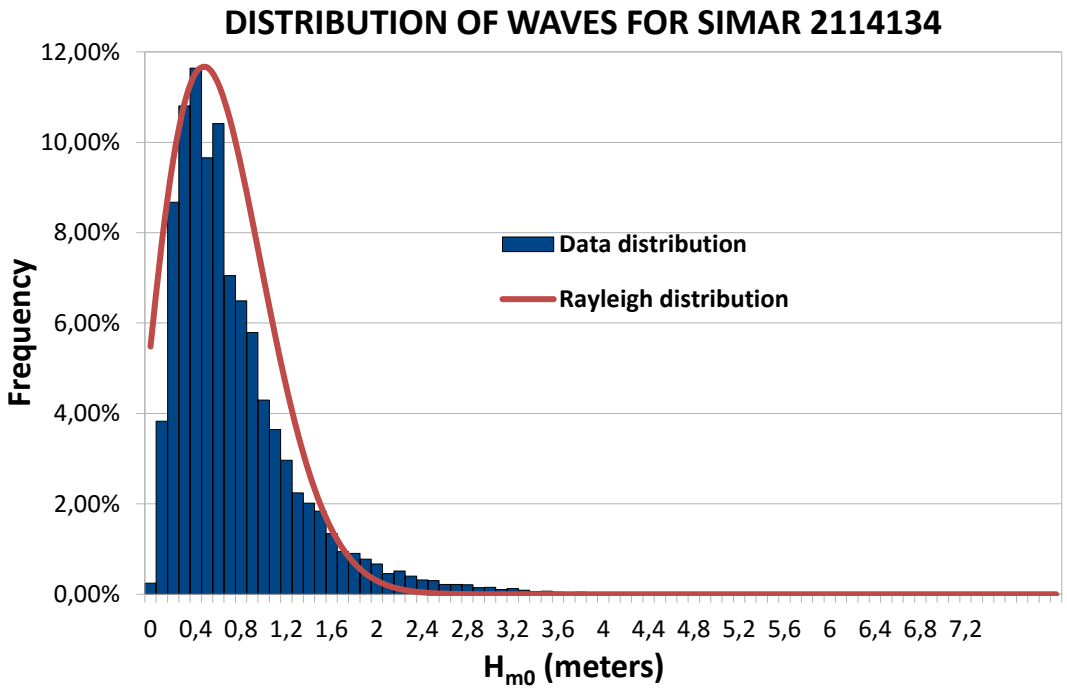

Figure 50: Histogram of wave height frequencies for SIMAR 2114134 and its adjusted Rayleigh distribution

The Rayleigh function or density function, is expressed as:

$$p(H) = \frac{2H}{H_{rms}^2} * e^{-\left(\frac{H}{H_{rms}}\right)^2}$$

where $p(H)$ is the probability of occurrence of the event H, and H_{rms} is the root-mean-square wave height, defined as:

$$H_{rms} = \sqrt{\frac{\sum_{i=1}^{N} H_i^2}{N}}$$

being H_i, the ith wave height value of the total N waves of data.

The integration of the function of Rayleigh derives to the probability distribution function $P(H)$, which defines the percentage of waves that have a height of less than

or equal to H. However from the point of view of our study and an engineering interpretation, it is more appropriate to speak in terms of probability of exceedance, in other words that is the percentage of waves having a wave height greater than a certain value of H. Therefore, the expression remains:

$$q = 1 - P(H) = e^{-\left(\frac{H}{H_{rms}}\right)^2}$$

In order to characterize the total set of data to a single value, a very representative wave parameter is the significant wave height H_s or $H_{1/3}$. The significant wave height is the arithmetic mean of the third highest waves of all the group of N waves. Knowing that the average wave height of any probability is expressed as the following relation, we can determine the significant wave height:

$$H_{\frac{1}{n}} = \frac{\int_{H_{1/n}}^{\infty} P(H) H dH}{\int_{H_{1/n}}^{\infty} P(H) dH}$$

And the significant wave height can be calculated by:

$$H_{\frac{1}{3}} = \sqrt{2} * H_{rms}$$

There is also the need to define in a single and representative value the other two main variables of the incident wave. After determining the significant wave height as a generic and unique value for the wave height, we can directly calculate a period *T* and a wavelength L_0, which would be the arithmetic average of the periods and wavelengths associated with the third highest waves.

11.1.2 Fall Velocity of Sediment Particles

When analyzing sediment transport, the estimation of the fall velocity of sediment particles, often called the settling velocity, is a fundamental requisite. The fall velocity is a downward velocity, combination between the gravity force, buoyancy force and fluid drag force, therefore it depends on the density and viscosity of the fluid but also on the size, shape and density of the sediment particle.

Over the last century a large number of relations for different particle sizes and different conditions were found in order to estimate the fall velocity. Many attempts have been carried out but still these relations have particular limitations when they are

used for engineering works. Some might be only applicable to spherical particles and it's not clear which relation is the most appropriate. Assuming the lack of such a solution, some laboratory investigations have been redirected to provide design curves to estimate the fall velocity of sediment particles based merely on the diameter of standard particles.

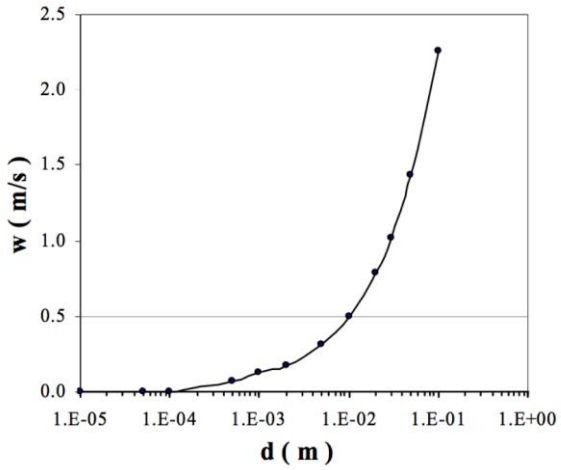

Figure 51: Mean Fall velocity for different particle sizes. ***Font: Sadat-Helbar, S. M., Darby, S. et al., 2009. Proceedings of the 4th IASME / WSEAS Int. Conference on WATER RESOURCES, HYDRAULICS & HYDROLOGY (WHH'09), Fall Velocity of Sediment Particles***

In 1851, Stokes investigated the coefficient of drag applied upon a spherical particle throughout the Navier-Stokes equations and a continuity equation expressed in polar coordinates. Stokes' results determined the fall velocity of spherical particles, assuming a region of the particle Reynolds number, *Re*, less than 1, calculated as:

$$w = \frac{1}{18}\,\frac{g(s-1)\,d(50)^2}{\upsilon}$$

where, *w* is the fall velocity of the sediment particle in m/s, *g* is the acceleration due to gravity in m/s^2, *d(50)* the particle diameter in m, υ the kinematic viscosity in m^2/s and *s* is the relative density defined as ρ_s/ρ, in which ρ_s and ρ are the density of the sediment and fluid in kg/m^3, respectively.

Similar equations and relations where found for natural sediment particles, but with some difficult issues due to the extensive variation of natural particle geometry. Therefore, different relations are presented exclusively applied within a limited range of fluid conditions or sediment characteristics.

In the table 3 below, we can see the expressions given by Hallermeier (1981) and Van Rijn (1989), as the Stokes one, to obtain the fall velocity of the natural sediment particles, under certain conditions. The relations are also shown as a combination of particle Reynolds number, *Re*, and the effective diameter, D_{gr}, described as:

$$Re = \frac{w * d}{\nu}$$

$$D_{gr} = d\left(\frac{g(s-1)}{\nu^2}\right)^{1/3}$$

ORIGINATOR	MAIN RELATION	MODIFIED RELATION	COMMENTS
Stokes (1851)	$w = \frac{1}{18}\frac{g(s-1)\,d(50)^2}{\upsilon}$	$Re = \frac{D_{gr}^3}{18}$	
Hallermeier (1981)	$Re = \frac{D_{gr}^3}{18}$ $Re = \frac{D_{gr}^{2,1}}{6}$ $Re = 1{,}05\,D_{gr}^{1,5}$	$Re = \frac{D_{gr}^3}{18}$ $Re = \frac{D_{gr}^{2,1}}{6}$ $Re = 1{,}05\,D_{gr}^{1,5}$	$D_{gr} < 3{,}42$ $3{,}42 < D_{gr} < 21{,}54$ $D_{gr} > 21{,}54$
Van Rijn (1989)	$w = \frac{1}{18}\frac{g(s-1)\,d(50)^2}{\upsilon}$ $w = 1{,}1\sqrt{[(s-1)gd]}$ $w = 10\frac{\upsilon}{d}\sqrt{1+0{,}01d^3}$	$Re = \frac{D_{gr}^3}{18}$ $Re = 1{,}1\,D_{gr}^{1,5}$ $Re = 10\,(\left(1+0{,}01D_{gr}^3\right)^{0{,}5} - 1)$	$d < 0{,}01\ cm$ $d > 0{,}1\ cm$ $d = 0{,}1\ cm$

Table 6: List of relations for estimating Fall velocity. ***Font: Sadat-Helbar, S. M., Darby, S. et al., 2009. Proceedings of the 4th IASME / WSEAS Int. Conference on WATER RESOURCES, HYDRAULICS & HYDROLOGY (WHH'09), Fall Velocity of Sediment Particles***

11.2 Generic Results and Discussions

The first step of the calculus is to determine the 3 main variables of the incident wave, $H_{1/3}$, $T_{1/3}$ and $L_{1/3}$ corresponding to the average wave height, period and wavelength of the third highest waves. For it, as we divided the Catalan coast into 8 well-differentiated zones with different data, we have to calculate those values for each region:

SIMAR	$H_{1/3}$ (m)	$T_{1/3}$ (s)	$L_{1/3}$ (m)
2098128	1,220709431	5,824549372	57,69226797
2098130	1,095107402	5,819964419	57,71101203
2104132	1,109890447	6,032752851	61,20138897
2114134	1,34462418	6,415427612	67,89922279
2118136	1,41306738	6,43468688	67,92407254
2124140	1,672210922	6,233719278	63,19269443
2126146	1,677129478	5,877276624	56,62351962
2128148	1,777427302	5,800564239	55,16180953

Table 7: Values of significant wave height $H_{1/3}$, and its associated significant period $T_{1/3}$ and wavelength $L_{1/3}$, for every SIMAR point

Many conclusions, already seen in the data analysis, can be checked on this table. As we argued for the mean values of every SIMAR point, although the high coefficient of variation values were not appropriately enough to work with, but above all, as we discussed with the different Fourier amplitudes and through the seasonal data analyses, wave tend to grow in height as we go further north. This growth in the north of Catalonia was associated to the proximity of the Gulf of Lion and the continuous and repetitive wind storms that affect the area. On the other hand, the period and thus the wavelength, since they are related as $\boldsymbol{L_0 = gT^2/2\pi}$, have their highest point on the intermediate SIMAR points, located on the central coast in front of the Barcelona's seaside.

Once the H1/3, T1/3 and L1/3 for every SIMAR point are established and the fall velocity wf for every beach, function of the grain size, is calculated, we are able to analyze the capacity of recovery of the beaches of the Catalan coast, throughout the analysis of cross-shore sediment transport indicators. 5 different parameters were chosen in order to estimate the landward or seaward sediment transport:

Parameter	Formula	Discrimination Value	
		Accretive	Erosive
Dean's Number	$\Omega = \frac{H_0}{w_f T}$	$\Omega < 2.8$	$\Omega > 2.8$
Hattori and Kawamata	$HK = \frac{2H_0}{w_s(d_{50})\,T}\ tan\beta$	$HK < 0{,}5$	$HK > 0{,}5$
Sunamura and Horikawa	$\frac{H_0}{L_0} = C(tan\beta)^{-0{,}27}\left(\frac{d}{L_0}\right)^{0.67}$	$C < 18$	$C > 18$
Ahrens' Criteria	$Ah = N_S\left(\frac{H_{SO}}{L_0}\right)^{0.854} e^{-10.1\left(\frac{H_{SO}}{L_0}\right)}$	$Ah < 30.8$	$Ah > 30.8$
Dalrymple's Profile Parameter	$P = \frac{gH_o^2}{w_f^3 T}$	$P < 10000$	$P > 10000$

Table 8: Definition of predictor parameters and their typical discrimination value

To be able to analyze also the complex calculus of the fall velocity, we proposed two ways of calculating it, by the Hallermeir method suggested in 1981 and by the latter Van Rijn method, 1989. Consequently the cross-shore sediment transport parameters of Dean's Number, Hattori and Kawamata and Dalrymple's profile parameter, the ones depending on the fall velocity, are calculated twice, for each settling velocity. To determine the calculation of the sediment particle fall velocity and the estimation of the 5 parameters, a sediment and seawater density of 2650kg/m3 and 1030kg/m3, respectively, have been taken into account. Moreover, for the computation of the Hallermeier's fall velocity, the viscosity parameter ν has been assumed to be constant with a value of 10^{-6} m^2/s, whereas for Van Rijn the viscosity is a variable depending on the following formula, supposing an average temperature of 20ºC:

$$\nu\ (m^2/s) = \left[\left(1{,}14 - 0{,}031 * (ºC - 15)\right) + (0{,}000068 * (ºC - 15)^2\right] * 10^{-6}$$

The first accretive or erosive results of the 390 beaches that compound the Catalan coast and for the 8 different parameters, are presented on the table below:

	ACCRETIVE	EROSIVE	MISSING VALUES	% OF ACCRETIVE	% OF EROSIVE
DEAN'S NUMBER	147	199	44	42,49%	57,51%
DEAN'S NUMBER (VAN RIJN)	150	196	44	43,35%	56,65%
HATTORI AND KAWAMATA	66	269	55	19,70%	80,30%
HATTORI AND KAWAMATA (VAN RIJN)	75	260	55	22,39%	77,61%
SUNAMURA AND HORIKAWA	65	270	55	19,40%	80,60%
DALRYMPLE	168	178	44	48,55%	51,45%
DALRYMPLE (VAN RIJN)	176	170	44	50,87%	49,13%
AHRENS CRITERIA	105	241	44	30,35%	69,65%
	119	**222,875**		34,64%	65,36%

Table 9: Accretive or erosive results of the 390 beaches of the Catalan coast for every parameter

Results have been colored with a gradient of colors in order to make it easier to see the differences between parameters, representing the highest number of accretive beaches in green and the lowest in red, per contra, the erosive beaches had been colored in green for the lowest number and red for the highest. An average of all the parameter results is also shown, as well as a column of the number of beaches that have missing values of data, whether it is because of a lack of the particle sizes of the beach, as would be the 44 cases of each of the parameters, or a lack of beach slope values, representing the 11 more cases that are added to the parameters of Hattori and Kawamata and Sunamura and Horikawa, those two that depend on the $tan\beta$. Finally, 2 very representative columns had been added, showing the accretive and erosive percentage upon the totality of beaches of the different parameters' results.

The first conclusion to be drawn is that parameters calculated by Van Rijn's fall velocity are more permissive and derive to higher accretive results, since values of the settle velocity are generally and slightly greater than the ones coming from the Hallermeier's formula. Otherwise, and helped by the gradient colored cells, it is clear that Dalrymple's profile parameter marks an accretive tendency with over than 50% of accretive beaches, followed by Dean's Number giving accretive results for more than 40% and in a midpoint is found the Ahrens Criteria parameter with almost a third of the Catalan coast accretive outcomes. Regarding Hattori and Kawamata and Sunamura and Horikawa, indicator specifically dependent on the slope stability, they give some results more erosive than the average, hardly reaching a 20% of accretive beaches.

Based on the average values, we can see that the closest indicators are Ahrens and Dean, both slightly below and above respectively. However, we note that Hattori and Kawamata and Sunamura and Horikawa have 11 more missing values than the rest, due to the absence of some beach slope data. We also know that those two parameters are based on empirical studies and charts, where a transition zone of accretive and erosive values is interpreted. Therefore, the large number of results that are close to the thresholds may be in that mentioned transition zone, and are counted as erosive although they could be accretive. For this conclusion, the number of accretive outcomes for this two indicators could be increased, implying a slight growth of the average, getting closer to the Dean's Number results and reaffirming that this parameter is the most overarching.

Finally, the last deduction that we can extract from the general results is related to the already mentioned difference of the wave heights depending on the location. As we go north the waves tend to be more energetic which would make us think that the highest concentration of erosive beaches would be in the north coast, although it is

not like that. In this thought the beach particle size is also involved and the larger the particle, the more resistance to strong waves. Below, a table showing the number of accretive beaches per SIMAR point and the percentage in that SIMAR area or over the total, and the mean granulometry and wave height, let us see the relation between $d_{50}/H_{1/3}$ and the amount of successful events:

SIMAR	$H_{1/3}$	d_{50}	$d_{50}/H_{1/3}$	Nº ACCRETIVE BEACHES	% SIMAR	% TOTAL
2098128	1,221	0,269	0,22014911	1,375	6,25%	0,40%
2098130	1,095	0,558	0,509244825	32,25	36,24%	9,32%
2104132	1,110	0,227	0,204483695	1	1,75%	0,29%
2114134	1,345	0,622	0,462680642	13	34,21%	3,76%
2118136	1,413	1,190	0,84240557	38,875	70,68%	11,24%
2124140	1,672	1,222	0,730661172	21,875	59,12%	6,32%
2126146	1,677	0,621	0,370514227	5,625	18,15%	1,63%
2128148	1,777	0,471	0,264748787	5	29,41%	1,45%
						34,39%

Table 10: Accretive results and relationship between significant wave height H1/3 and mean grain size d50 for every SIMAR point

With the table above we can rule out that the wave height is not the only general characteristic that determine the amount of erosive or accretive beaches, and that we also have to take into account the grain size. It demonstrates that where the relationship between particle size and wave height is closer to 1, that is, where there are coarser grains of sand, there will be more accretive resulting beaches. Therefore, it can be highlighted that although the Costa Brava is hit by constant bigger waves, the percentage of erosive beaches is not as high as expected since the mean granulometry is quite thick. Instead, for the southern places, where the waves have less energy, the number of accretive beaches is extremely low, due to a small average diameter of the particles and consequently a low ratio of d50/H1/3.

11.2.1 Evaluation of Results of Each Parameter

To interpret in a different way the results, it may be interesting also to do a distribution and statistical analysis of the outcoming values for each parameter indicator. Such analyzes can be performed with the help of histograms or with the study of the statistics variables of distribution, easily visible on box-plots, representing numerical data through their quartiles.

11.2.1.1 Dean's Number Parameter

As we have proven, Dean's parameter is the closest of all to the average, so it is considered the most representative parameter for the study of the cross-shore sediment transport. The result of applying the formula is a dimensionless variable, which defines the direction of the sediment transport at the threshold value of 2.8. If the value given is less than the limit value, the sediment is moving toward the land, whereas if it is higher, it corresponds to a seaward-directed transport. The results for both, the Hallermeier and the Van Rijn fall velocity, have been plotted by their frequency of appearance and regrouped by bins with a difference of 0,3.

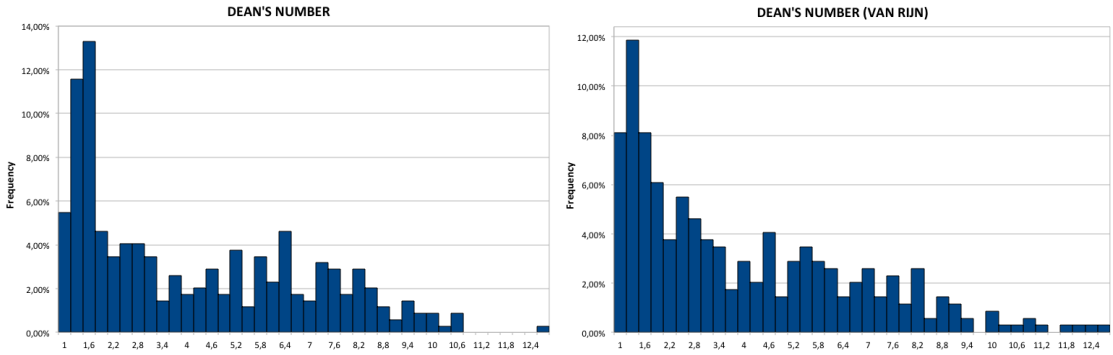

Figure 52: Histograms for Dean's Number. For Hallermeier fall velocity on the left and Van Rijn on the right

Regarding the results for Hallermeier, there is a large accumulation of results for values below the Dean's threshold, with a frequency peak of over 13% of the total results. However, it also appears another peak for higher values, less defined this time, corresponding to the Dean value around 6 with a frequency of 4%, relatively lower than the main accumulation peak.

A priori the results for Van Rijn are very similar to the previous ones, but they present a small trend toward the left of the whole results data. As we discussed and as it was expected, the falling velocity of Van Rijn was generally higher than the one calculated by Hallermeier's formulas, which provides lowest values of the parameters since they are inversely proportional to the settling velocity.

In order to study the histograms' difficult configuration we tried to identify them with any known distribution function. For that purpose, we analyzed the data set with EasyFit, a distribution-fitting program made by Mathwave Technologies. The reverse J-shaped distributions of Dean's Number results, for Hallermeier's and Van Rijn's particle fall velocity, were fitted as a Johnson SB and a Dagum probability density distributions respectively, with the following parameters:

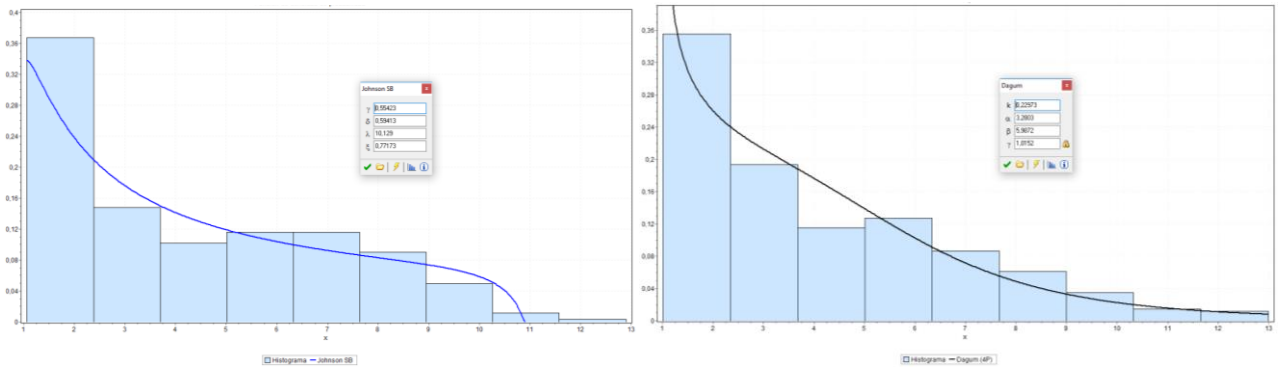

Figure 53: Deans's histograms fitted as Johnson SB (0,55; 0,59; 10,129; 0,77) and Dagum (0,23; 3,29; 5,99; 1,015)

Being the Johnson SB probability density function as follows:

In the domain $\xi \leq H \leq \xi + \lambda$:

$$f(H) = \frac{\delta}{\lambda\sqrt{2\pi}H(1-H)} e^{\left(-\frac{1}{2}\left(\gamma+\delta\ln\left(\frac{H}{1-H}\right)\right)^2\right)}$$

And the Dagum distribution:

In the domain $\gamma \leq H \leq +\infty$:

$$f(H) = \frac{\propto k\left(\frac{H-\gamma}{\beta}\right)^{\propto k-1}}{\beta\left(1+\left(\frac{H-\gamma}{\beta}\right)^{\propto}\right)^{k+1}}$$

The fact that the peak frequency is below the limit value of Dean does not mean that more than a half of the values are underneath it. Consequently it becomes important the study of quartiles and box-plot representation. The quartiles of a set of data values are the three points that divide the data set into four equal groups, each group comprising a quarter of the data. Therefore the first quartile, splits off the lowest 25% of data from the highest 75%, the third splits off the highest 25% of data from the lowest 75%, and the second, known as the median is the group that divides in half the total values of the data set. With the calculation of quartiles, as well as other statistic variables presented below, we are able to draw a box-plot:

	DEAN'S	DEAN'S (VAN RIJN)
Minimum	1,064	1,015
Quartile 1	1,722	1,788
Median	3,409	3,296
Quartile 3	6,472	5,924
Maximum	12,894	12,987
Mean	4,301	4,131
Variance	7,494	7,307
Standard Deviation	2,737	2,703
Variation Coefficient	0,637	0,654
Mode	1,668	1,592
Threshold	**2,8**	

Table 11: Main statistic variables

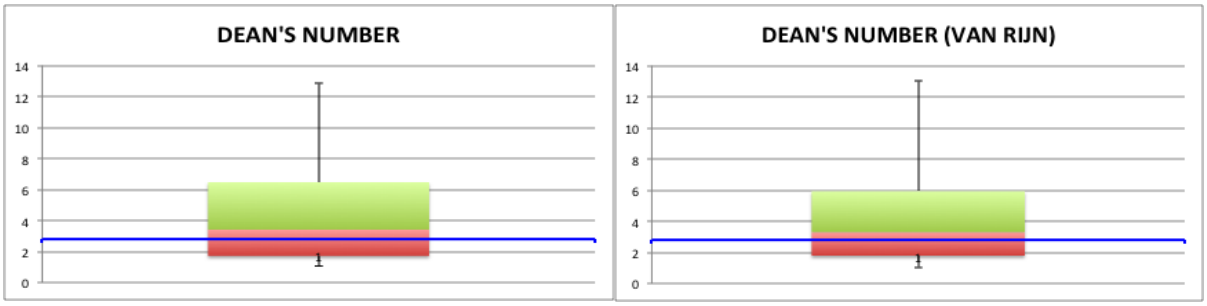

Figure 54: Box-plots for Dean's Number. For Hallermeier fall velocity on the left and Van Rijn on the right

The green box is the one corresponding to the third quarter of values and the red one to the second quarter. A blue line has been drawn to identify the threshold value of 2,8, in that way it is easier to see the percentage of outcomes that are above or below it. With the main statistic values and their representation on the box-plots we realize that slightly less than half of the values are above the limit value, although it may not look like in the histograms, therefore Dean indicates that there are vaguely more erosive results, as we already discussed earlier. The variation coefficient is a little bit high due to a wide domain of values and an upper extreme value far from the median.

11.2.1.2 Hattori and Kawamata Parameter

Hattori and Kawamata defined a dimensionless sediment transport parameter with a limit value of 0,5, representing a landward transport for lower values and a seaward-directed transport instead. The results for both, the Hallermeier and the Van Rijn fall velocity, have been plotted by their frequency of appearance and regrouped by bins with a difference of 0,1.

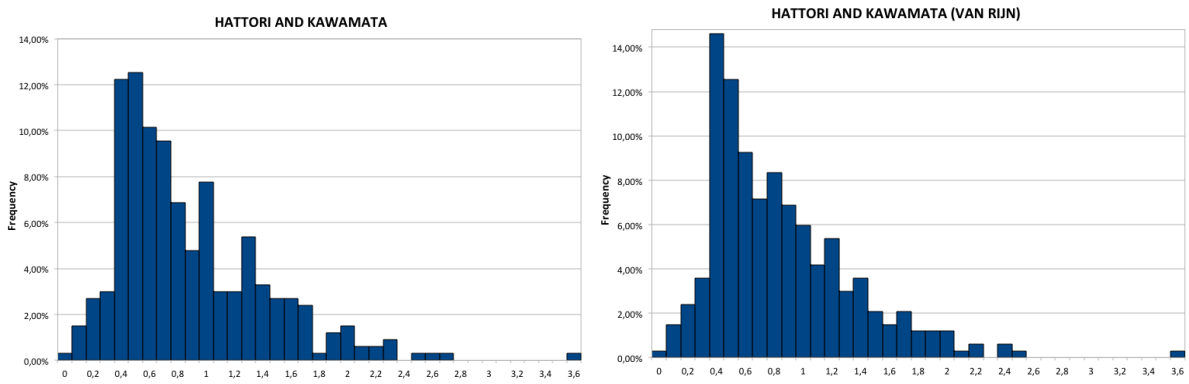

Figure 55: Histograms for Hattori and Kawamata parameter. For Hallermeier fall velocity on the left and Van Rijn on the right

The results are very similar depending on the fall velocity used, but again they present a small trend toward the left of the whole set of data, due to the generally higher results for Van Rijn's falling velocity providing lower values of the parameters. The pick of frequencies is found in low bin values being higher than 12% for 0,4 to 0,5 bin and 0,5 to 0,6. The histograms are typical right-skewed bell-shaped distributions and have been approximated, with the EasyFit program, to an Inverse Gaussian for Hallermeier's results and a Log-Logistic for Van Rijn.

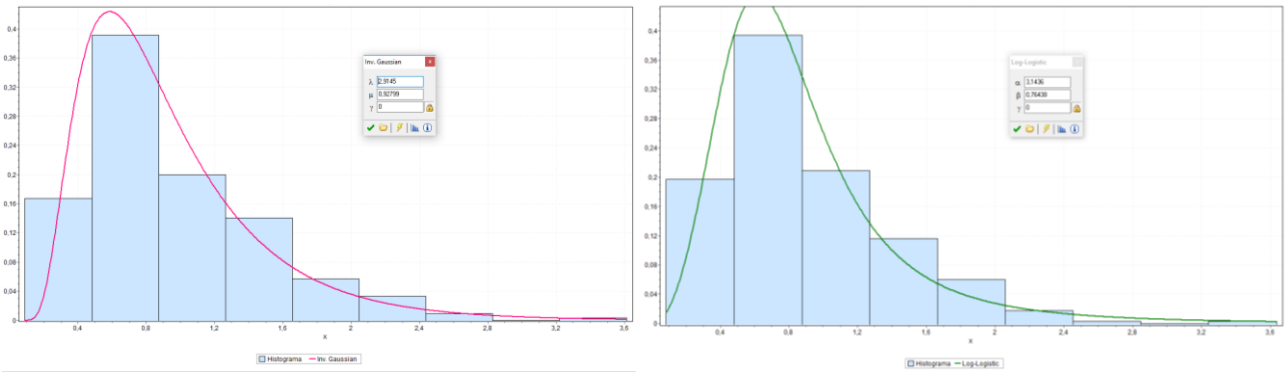

Figure 56: Hattori and Kawamata's histograms fitted as Inv. Gaussian (2,91; 0,93) and Log-Logistic (3,14; 0,76)

Being the Inv. Gaussian probability density function as follows:

In the domain $0 \leq H \leq +\infty$: $$f(H) = \sqrt{\frac{\lambda}{2\pi H^3}} e^{-\frac{\lambda(H-\mu)^2}{2\mu^2 H}}$$

And the Log-Logistic distribution:

In the domain $0 \leq H \leq +\infty$: $$f(H) = \frac{\alpha}{\beta}\left(\frac{H-\gamma}{\beta}\right)^{\propto-1}\left(1+\left(\frac{H-\gamma}{\beta}\right)^{\propto}\right)^{-2}$$

Again with the calculation of quartiles, as well as other statistic variables presented below, we are able to draw a box-plot:

	HATTORI AND KAWAMATA	HATTORI AND KAWAMATA (VAN RIJN)
Minimum	0,090	0,086
Quartile 1	0,538	0,514
Median	0,775	0,778
Quartile 3	1,213	1,160
Maximum	3,610	3,636
Mean	0,928	0,891
Variance	0,274	0,245
Standard Deviation	0,524	0,495
Variation Coefficient	0,564	0,555
Mode	0,600	0,573
Threshold	**0,5**	

Table 12: Main statistic variables

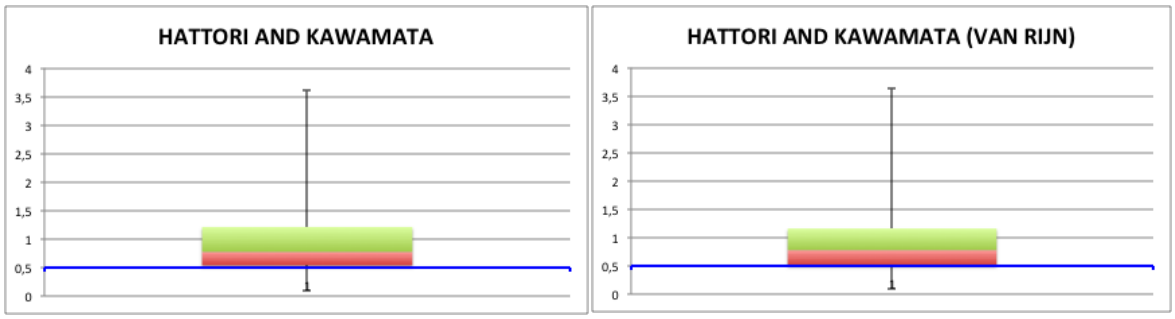

Figure 57: Box-plots for Hattori and Kawamata. For Hallermeier fall velocity on the left and Van Rijn on the right

The blue line represents the threshold value of 0.5, in that way it is easier to see the percentage of outcomes that are above or below it. With the main statistic values and their representation on the box-plots we realize that slightly less than the first quartile of the values are below the limit value, which means that there are vaguely more than 75% of erosive results, as we already saw earlier. The mean and mode values are above the threshold and the upper maximum value is far from the green and red boxes, representing the second and third quartiles, from the 25% to the 75% of the outcomes.

11.2.1.3 Sunamura and Horikawa Parameter

For Sunamura and Horikawa the dimensionless results where plotted through bins of 2 points wide, and presents the following form:

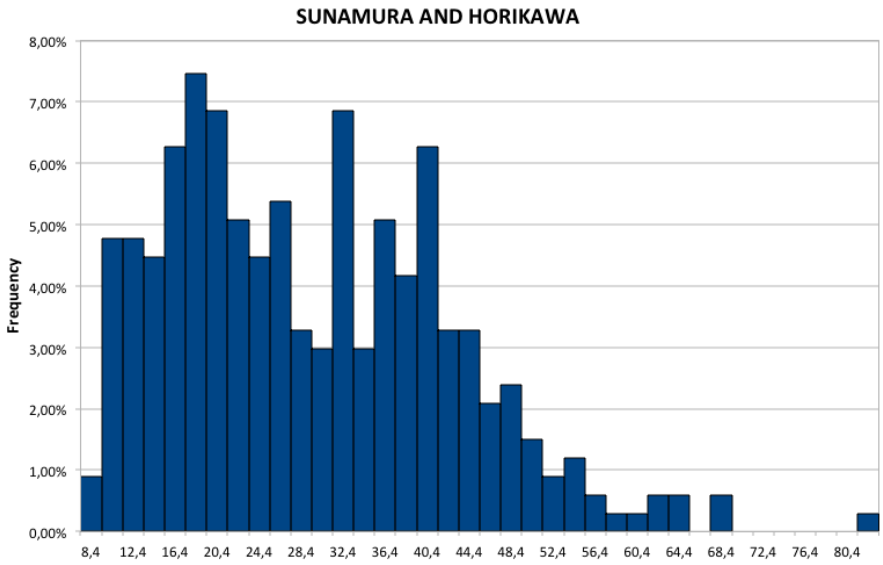

Figure 58: Histogram for Sunamura and Horikawa parameter

This time, the histogram show a very peculiar configuration and it is kind of difficult to identify it with any known distribution function. The frequency peaks are scattered throughout the domain and therefore it is not recognizable to any known distribution function or shape. Being so difficult to evaluate the histogram, we can calculate some of the most important statistical values with which we will be able to create a box-plot diagram:

	SUNAMURA AND HORIKAWA
Minimum	8,411
Quartile 1	19,559
Median	28,060
Quartile 3	40,022
Maximum	82,811
Mean	30,252
Variance	176,868
Standard Deviation	13,299
Variation Coefficient	0,440
Mode	15,808
Threshold	**18**

Table 13: Main statistical variables

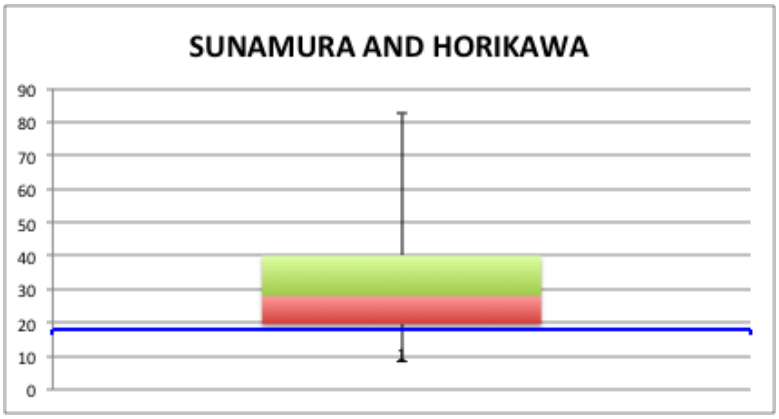

Figure 59: Box-plot for Sunamura and Horikawa

Vaguely more than three quarters of the outcomes are above the limit value of 18, represented as the blue line. Even so, the mode value is below meaning that the highest density of frequency of results is beneath the threshold, which agrees with the histogram. As to the mean it is way above the limit which, knowing that the mode is below, let us quantify the spread of the results throughout their domain.

11.2.1.4 Dalrymple's Profile Parameter

The Dalrymple's parameter histograms, with a limit value of 10000, for both ways of calculating the fall velocities are represented below with bins of 12000 points each, but with an initial bin comprising values from 0 to the threshold:

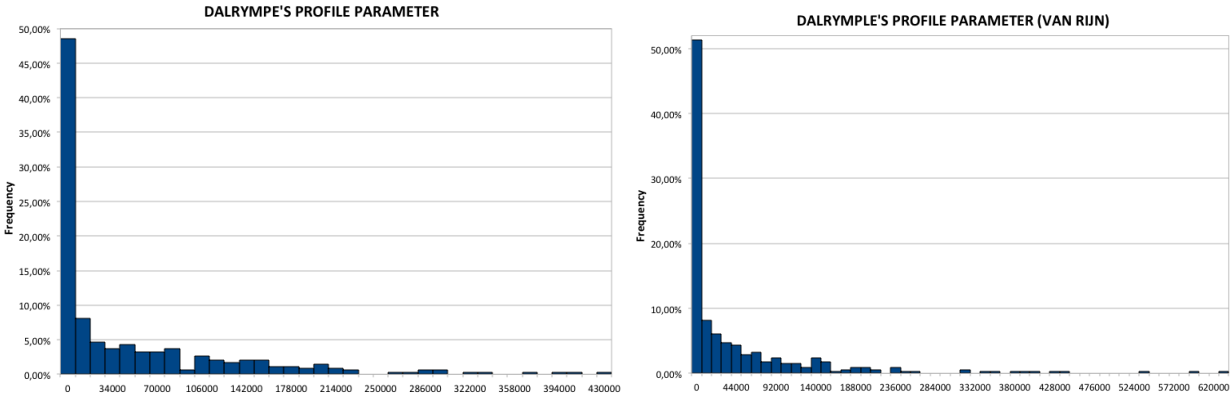

Figure 60: Histograms for Dalrymple's parameter. For Hallermeier fall velocity on the left and Van Rijn on the right

Both histograms present a really well defined reverse J-shape, with a unique peak in the first bin which consists on the below threshold values. This peak supposes almost the 50% for the Hallermeier's results and overcomes it for Van Rijn, since as we already discussed, higher fall velocities push resulting values to the left and tend to accumulate them on lower bins.

Both histograms were identified and fitted as Birnbaum–Saunders distributions, also known as the fatigue life distribution, with the following parameters:

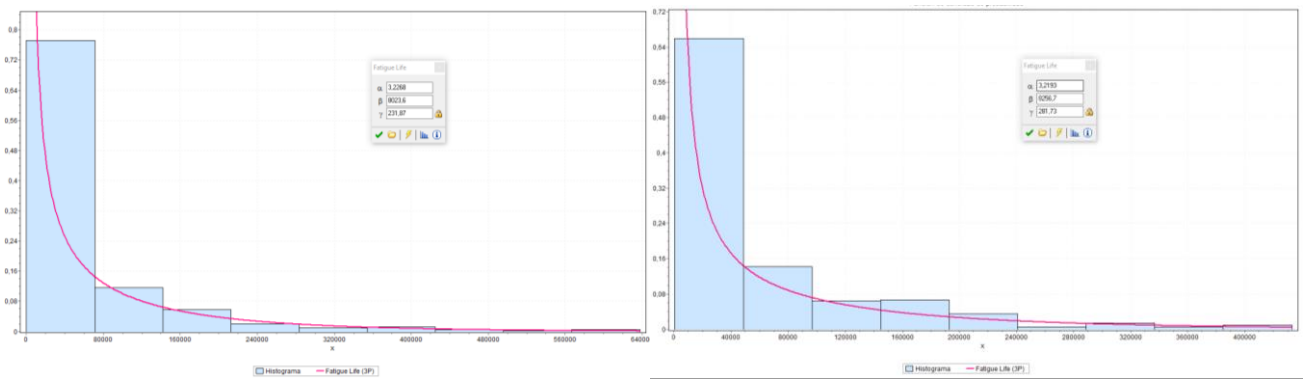

Figure 61: Dalrymple's histograms fitted as Fatigue Life (3,23; 8023,6; 231,9) and (3,22; 8256,7; 281,73)

Being the Fatigue Life probability density function as follows:

In the domain $\gamma \leq H \leq +\infty$: $$f(H) = \frac{\sqrt{(H-\gamma)/\beta}+\sqrt{\beta/(H-\gamma)}}{2\propto(H-\gamma)} * \emptyset\left(\frac{1}{\propto}\sqrt{\frac{(H-\gamma)}{\beta}} - \sqrt{\frac{\beta}{(H-\gamma)}}\right)$$

Although results are much clear with this parameter, the main statistical values have been calculated and the box-plots have been plotted:

	DALRYMPLE'S	DALRYMPLE'S (VAN RIJN)
Minimum	365,046	317,495
Quartile 1	1321,250	1294,786
Median	11546,431	9030,613
Quartile 3	80449,981	59315,894
Maximum	433097,299	637451,590
Mean	53664,034	51552,935
Variance	6410101982,310	8762474082,767
Standard Deviation	80063,112	93608,088
Variation Coefficient	1,492	1,816
Mode	1334,080	1160,304
Threshold	**10000**	

Table 14: Main statistical variables

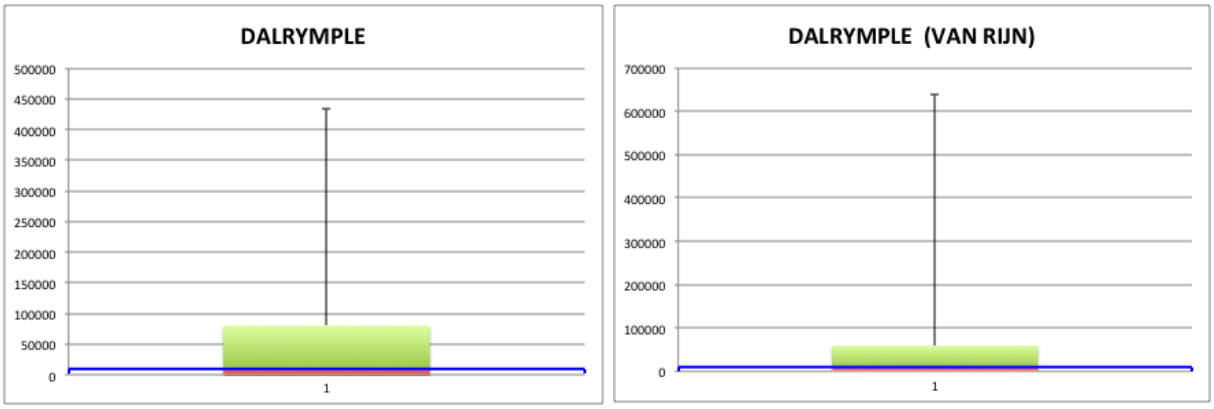

Figure 62: Box-plots for Dalrymple's parameter. For Hallermeier fall velocity on the left and Van Rijn on the right

We can see that the blue line delimiting the threshold value is around the median and therefore nearby 50% of the results for Dalrymple's parameter are accretive, as we already discussed. The red box, representing the second quartile of values, is really low meaning that the first half of outcomes are really concentrated in low values, below 10000, while the rest are spread out through the whole domain arriving until 433097 points. This is also seen with the statistical variables, since the mean is way above the threshold and, although the majority of values are not, the mode, the most repeated ones, is slightly above too.

11.2.1.5 Ahrens Criteria

For Ahrens Criteria parameter the dimensionless results where plotted through bins of 6 points wide, and presents the following form:

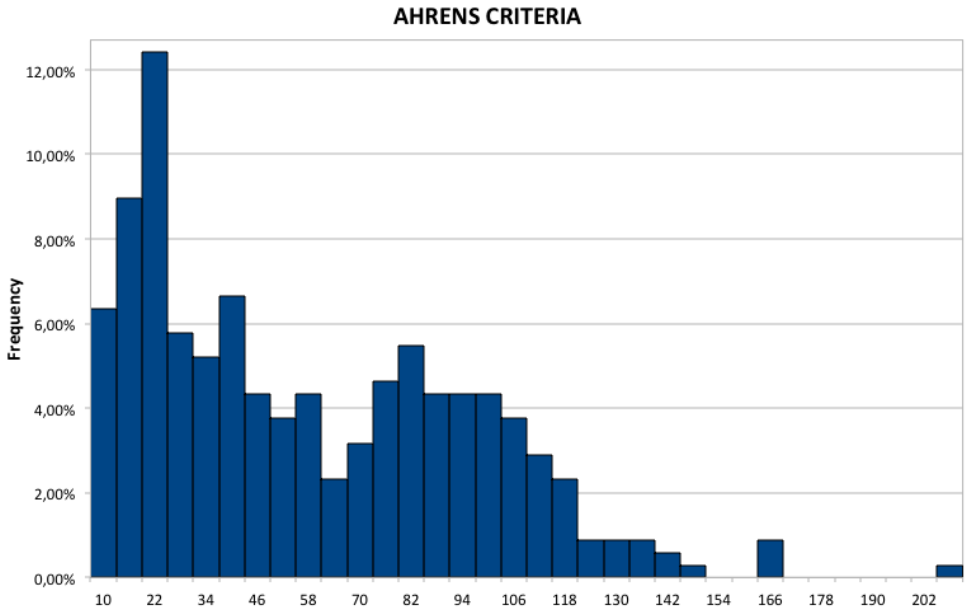

Figure 63: Histogram for Ahrens Criteria parameter

The frequency distribution of the Ahrens Criteria results show a very irregular configuration and it is problematic to identify it with any known distribution function. The histogram presents two main accumulation of values, one short range with high frequency for the lowest outcomes around 16 to 28 and the other quite wide but with less frequencies for each bin for higher results throughout 76 to 106 points.

As we can not recognize any know distribution function, we may analyze some of the most common statistics variables and plot them:

	AHRENS
Minimum	10,576
Quartile 1	26,192
Median	52,581
Quartile 3	89,500
Maximum	212,741
Mean	60,910
Variance	1431,573
Standard Deviation	37,836
Variation Coefficient	0,621
Mode	26,169
Threshold	**30,8**

Table 15: Main statistical variables

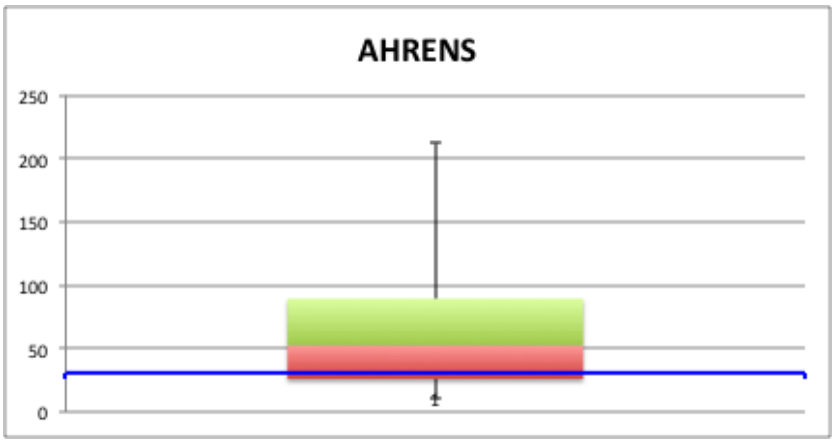

Figure 64: Box-plot for Ahrens Criteria

Vaguely more than one quarter of the outcomes are below the limit value of 30,8, represented as the blue line, which mean there are over 25% of accretive results. Even so, the mode value is below meaning that the highest density of frequency of results is beneath the threshold, which agrees with the histogram. As to the mean it is way above the limit which, knowing that the mode is below, let us quantify the spread of the results throughout their domain.

11.3 Seasonal and Directional Results and Discussions

As we did with the data analysis, it might be interesting to analyze also the results through the different seasons or the 4 main wind direction origins. The numbers of accretive and erosive beaches for each of the 8 parameters of study are shown on the tables on the next page, as well as an average value and the percentage upon the total 346 number of beaches. In fact, another table showing the number of missing values per lack of data is added, since actually the number of beaches of study was 390. Below we can also see a table with the significant wave height $H_{1/3}$ for every SIMAR point and every case of study:

SIMAR	WINTER	SUMMER	N	E	S	W
2098128	1,330	0,816	1,263	1,396	1,072	1,108
2098130	1,189	0,748	1,019	1,291	0,971	1,085
2104132	1,210	0,735	1,116	1,108	1,113	1,104
2114134	1,474	0,851	1,356	1,324	1,347	1,434
2118136	1,547	0,904	1,054	1,825	1,066	1,097
2124140	1,816	1,142	2,039	2,208	1,066	0,882
2126146	1,816	1,170	1,487	2,345	1,125	0,918
2128148	1,922	1,255	1,522	2,439	1,232	1,006

Table 16: Significant wave height $H_{1/3}$ for every SIMAR and case of study

	NO DATA							
	DEAN	**DEAN VAN RIJN**	**H&K**	**H&K VAN DIJN**	**S&H**	**DALRYMPLE**	**DALRYMPLE VAN RIJN**	**AHRENS**
TOTAL	44	44	55	55	55	44	44	44
WINTER	44	44	55	55	55	44	44	44
SUMMER	44	44	55	55	55	44	44	44
N	44	44	55	55	55	44	44	44
E	44	44	55	55	55	44	44	44
S	44	44	55	55	55	44	44	44
W	44	44	55	55	55	44	44	44

Table 17: Number of no data beaches due to lack of grain size d_{50} or beach slope $tan\beta$

	ACCRETIVE									
	DEAN	DEAN VAN RIJN	H&K	H&K VAN DIJN	S&H	DALRYMPLE	DALRYMPLE VAN RIJN	AHRENS	MEAN	%
TOTAL	147	150	66	75	65	168	176	105	119	34,39%
WINTER	141	138	47	61	52	166	173	96	109,25	31,58%
SUMMER	174	184	120	124	137	189	199	166	161,625	46,71%
N	149	153	97	97	87	171	178	108	130	37,57%
E	136	135	36	43	45	156	162	73	98,25	28,40%
S	164	170	108	115	112	174	188	131	145,25	41,98%
W	155	157	104	108	115	173	183	131	140,75	40,68%

Table 18: Accretive results for each parameter and each case of study

	EROSIVE									
	DEAN	DEAN VAN RIJN	H&K	H&K VAN DIJN	S&H	DALRYMPLE	DALRYMPLE VAN RIJN	AHRENS	MEAN	%
TOTAL	199	196	269	260	270	178	170	241	222,875	64,41%
WINTER	205	208	288	274	283	180	173	250	232,625	67,23%
SUMMER	172	162	215	211	198	157	147	180	180,25	52,10%
N	197	193	238	238	248	175	168	238	211,875	61,24%
E	210	211	299	292	290	190	184	273	243,625	70,41%
S	182	176	227	220	223	172	158	215	196,625	56,83%
W	191	189	231	227	220	173	163	215	201,125	58,13%

Table 19: Erosive results for each parameter and each case of study

Logically, as it was expected, the results for Winter are way more erosive than in Summer. In fact, the latter one presents the highest values of accretive beaches of all the cases of study and thus the lowest values of erosive results. This is explained as the waves recorded in wintertime, as discussed above, are much more powerful and energetic, therefore they apply more force to the coast, producing more erosion profiles to the finer sand or steepest beaches, while summer is a mild energy season characterized by smaller waves.

At the data analysis we found out that the main and more energetic direction for practically all the Catalan coast was the East one, and although it was not the main in certain points, at least we realized that the wave distribution exposed us that it was an important direction concentrating high values of wave heights, periods and wavelengths. So as anticipated, the results are not disappointing and show us that this highly energetic direction concentrates a huge number of erosive profiles. In fact, it presents the lowest values of accretive beaches of all the cases of study and thus the highest values of erosive results, with over 70% of the beaches.

Analyzing data we also spotted that the North direction took quite a lot of importance in some points, which is why it is the second most energetic direction, presenting more than 60% of erosive outcomes. Regarding the last two directions, South and West, they grouped the mildest waves as we can see on the table 16, and their results are practically the same, being the former one the slightly more accretive of the two.

12. Final Conclusions

The objective of this project was to analyze the capacity of waves to induce an onshore/offshore sediment transport along the Catalan coast to evaluate the capacity of beaches to recover the original shape after the pass of an extreme event. Quantitative results have already been analyzed for the total set of data and for periods, such as considering only winter conditions or more favorable ones on summer, as well as evaluating the 4 main wave source directions.

The results for every specific beach can be found in the ANNEX, but anyway, we can draw some general conclusions on the behavior of the Catalan coast. First of all, it is important to underline the main relations that characterize the beach profile response and thus, the capacity of it to recover. Basically the results are controlled by the wave height *H*, the period *T* or the wavelength *L*, as for incident wave variables, and by the grain size d_{50} and the beach slope $tan\beta$, as for coast characteristics data.

It has been shown that the higher the wave height *H*, the more erosive outcomes. But we cannot analyze the wave height by its own, since there are other variables involved too, such as the grain size d50, defining a higher fall velocity the thicker the sediment and thus resulting in more accretive number of beaches, and also the longer the wavelength L, the longer the period *T*, which are directly related, and the more accretive positive results. That is why it is important to emphasize on their relations instead of looking at each variable alone.

The inverse relation of results between wave height and the rest of variables present the following ratios, for which the higher the more erosive: wave height related to the granulometry H/d_{50} and the wave steepness ratio *H/L* and its homonym *H/T*. Lastly, and only related to the Hattori and Kawamata and the Sunamura and Horikawa parameters, the beach slope also defines the required energy to move sediments and consequently, the higher $tan\beta$, the less energy needed and the more erosive outcomes.

Moreover, according to our analysis, we can conclude that the Dean's Number parameter is the closest to the average of all the calculated ones and therefore turns out to be the most reliable. Ahrens has also presented quite centered results even though it is a bit more restrictive with slightly lower accretive beaches results. Dalrymple's profile parameter instead, is more permissive and its outcomes result to be more accretive. Finally, Hattori and Kawamata and the Sunamura and Horikawa parameters are the most restrictive and so their results are way below the average.

To see the relevance of each one of them, on the table below we can see, for the eight parameters, the minimum, maximum and mean accretive results of all the cases

of study, which directly correspond to the summer on a seasonal analysis of data for the maximum and a minimum found on the directional study in the East direction:

	DEAN	DEAN VAN RIJN	H&K	H&K VAN RIJN	S&H	DALRYMPLE	DALRYMPLE VAN RIJN	AHRENS
MAX (*Summer*)	174	184	120	124	137	189	199	166
MEAN	152,43	155,43	84,29	90,57	87,57	171,00	179,86	115,71
MIN (*East*)	136	135	36	43	45	156	162	73
LOSS %	**21,84%**	**26,63%**	**70,00%**	**65,32%**	**67,15%**	**17,46%**	**18,59%**	**56,02%**

Table 20: Maximum (Summer), mean and minimum (East) accretive results of all cases of study

The percentage of loss between both values has also been calculated and surprisingly it is not uniform for every parameter. In fact, the loss percentage is related to the permissiveness of each one and for less restrictive parameters, such as Dalrymple or Dean, it is quite low, while for Hattori and Kawamata and the Sunamura and Horikawa parameters, the more restrictive, it reaches the 70% of loss. This large difference is explained by the accumulation of results near the limit value, which means that a small variation in any variable results in a significant fluctuation above and below the threshold.

Finally, we have seen the quantitative results through many different views of study, but we are missing a qualitative solution. The best way to do so is to divide the results according to the number of positive parameters, and so the following criteria was established:

	MEANING
≤ 4	Unlikely to happen or Impossible
> 4	Possible to happen
> 5	Likely to happen
> 6	Probable to happen
> 7	Certainly to happen

Table 21: Qualitative criteria

With this criterion we can finally quantify and qualify the erosive or accretive beaches of the Catalan coast. Results with less than the half of positive parameters are considered impossible to happen as well as having only 4 are considered unlikely, since Dean and Dalrymple, both the most accretive results permissive parameters, are calculated with Hallermeier's fall velocity and Van Rijn's, for which the statisctical expectation of having 3 or 4 positive values, comprising only Dean's parameters and Dalrymple's, is very high.

A simple accretive analysis for this qualitative results have been made, centralizing also at the three coastal areas of Catalonia, Tarragona, Barcelona and Girona:

	TOTAL	%	TGN	%	% TOTAL	BCN	%	% TOTAL	GIR	%	% TOTAL
>4	112	32,37%	29	21,97%	8,38%	39	37,14%	11,27%	44	44,90%	12,72%
>5	85	24,57%	28	21,21%	8,09%	38	36,19%	10,98%	19	19,39%	5,49%
>6	54	15,61%	23	17,42%	6,65%	16	15,24%	4,62%	15	15,31%	4,34%
>7	32	9,25%	17	12,88%	4,91%	10	9,52%	2,89%	5	5,10%	1,45%

Table 22: Accretive results for the qualitative analysis of the totality of beaches and centralizing the results in Tarragona, Barcelona or Girona

The results are clear, at most 112 beaches of the 346 of study, the 32.4%, have an accretive profile, the largest number of which is located in Girona with a 12.72% of the results, followed by Barcelona with 11,27% and finally Tarragona with the 8.38%. If we look at the local percentages for more than 4 positive indicators the results are practically the same, being Girona the location where the highest number of its beaches are accretive and Tarragona presenting the worst results in terms of accretive outcomes. However, considering likely to happen conditions or even more, Girona loses large number of beaches and therefore local percentage, which let us realize the big quantity of 5 positive indicators results. And for results that are certainly to happen, those with all the indicators positive, Tarragona is the location with most local percentage, followed by Barcelona and finally Girona, representing the 9.25% of the total beaches of the Catalan coast.

To sum up, the beaches with an erosion profile, those with four or fewer parameters that indicate a landward sediment transport, represent the 67.63%, a total of 234 beaches. In a very schematic way, the erosive profile beaches are concentrated in 4 main zones. From south to north, they are found in the *Delta del Ebre* itself, north of *Tarragona* city till the *Llobregat* river, coast of *Barcelona* city and *Maresme*, except for 8 almost consecutive results north of the *Besòs* river and finally from the beach of *Pals* throughout all the *Alt Empordà*, although we have to take into account that much of the null data beaches are found in the *Cap de Creus* region, 17 of the 44 to be exact.

13. REFERENCES

Ahrens, J.P., Hands, E.B., 1998. Parameterizing beach erosion/accretion conditions. 26th Int. Conf. on Coastal Engineering (1998), ASCE, 2382-2394.

Dalrymple, R.A., 1992. Prediction of storm/normal beach profiles. J. Waterway, Port, Coastal, Ocean Eng. 118 (1992) 193-200.

Dean, R.G., 1973. Heuristic model of sand transport in the surf zone, Proc. of Conf. on Engineering Dynamics in the Surf Zone, Sydney, 208-214.

Hattori, M., Kawamata, R., 1980. Onshore-Offshore transport and beach profile change. 17th Int. Conf. on Coastal Engineering (1980), ASCE, 1175-1193.

Kraus, N.C., Larson, M., Kriebel, D.L., 1991. Evaluation of beach erosion and accretion predictors. Coastal Sediments '91, 572-587.

Kriebel, D.L., Dally, W.R., Dean, R.G., 1986. Undistorted Froude Model for Surf Zone Sediment Transport, 20th Int. Conf. on Coastal Engineering (1986), ASCE, Taipei, 1296–1310.

Larson, M., Kraus, N.C., 1989. SBEACH: Numerical model for simulating storm induced beach change. Report 1: Empirical foundation and model development. Technical Report CERC-89-9.

Mariño-Tapia, I.J., Russel, P.E. et al., 2007. Cross-shore sediment transport on natural beaches and its relation to sandbar migration patterns. Journal of Geophysical Research, VOL. 112, C03001, doi: 10.1029/2005JC002893, 2007.

Nicholls, R. J., Larson, M., Capobianco, M. and Birkemeier, W.A. Depth of closure: Improving understanding and prediction.

Sadat-Helbar, S. M., Darby, S. et al., 2009. Proceedings of the 4th IASME / WSEAS Int. Conference on WATER RESOURCES, HYDRAULICS & HYDROLOGY (WHH'09), Fall Velocity of Sediment Particles, ISBN: 978-960-474-057-4, 39-45.

Sunamura, T., Horikawa, K., 1974. Two-dimensional beach transformation due to waves. 14th Int. Conf. on Coastal Engineering (1974), ASCE, 920-938.

Velinga, P., 1986. Beach and Dune Erosion during Storm Surges. Delft Hydraulics Communications No. 376.